# S-nitrosoglutathione reductase deficiency is associated with altered recovery from repeated climate stress across generations in *Arabidopsis thaliana*

**Running title:** NO homeostasis and multigenerational stress recovery

**Authors:** Behl R[1], Ghirardo A[1,2], Winkler JB[1,3], Jafarian S[4], Frungillo L[5], Spoel SH[5], Fischbach A[6], Huber G[6], Koller R[6], Albert A[1], Mattes E[7], Gößl L[4], F.X. Mayer K[4,8], Johannes F[9*], Lindermayr C[7,8*], Schnitzler JP[1,2,10*]

**Corresponding authors:** Johannes F[8*], Lindermayr C[7,8*], Schnitzler JP[1,2,9*]

**Affiliations:** [1] Research Unit Environmental Simulation (EUS), Helmholtz Munich, Neuherberg, Germany.

[2] Institute for Translational Metabolism Research, Helmholtz Diabetes Center, Helmholtz Munich / School of Medicine and Health, Technical University of Munich, Munich, Germany

[3] Institute of Plant Biology, Technische Universität Braunschweig, Germany

[4] Plant Genome and Systems Biology, Helmholtz Munich, Neuherberg, Germany.

[5] Institute of Molecular Plant Sciences, School of Biological Sciences, University of Edinburgh, Edinburgh EH9 3BF, UK.

[6] Institute of Bio- and Geosciences: Plant Sciences (IBG-2), Forschungszentrum Jülich GmbH, Jülich, Germany.

[7] Institute of Lung Health and Immunity (LHI), Comprehensive Pneumology Center (CPC-M), Helmholtz Munich, Neuherberg, Germany.

[8] TUM School of Life Sciences, Technical University Munich, Weihenstephan, Germany.

© The Author(s) 2026. Published by Oxford University Press on behalf of Society for Experimental Biology. This is an Open Access article distributed under the terms of the Creative Commons Attribution-NonCommercial-NoDerivs licence (https://creativecommons.org/licenses/by-nc-nd/4.0/), which permits non-commercial reproduction and distribution of the work, in any medium, provided the original work is not altered or transformed in any way, and that the work is properly cited. For commercial re-use, please contact reprints@oup.com for reprints and translation rights for reprints. All other permissions can be obtained through our RightsLink service via the Permissions link on the article page on our site—for further information please contact journals.permissions@oup.com.



ACCEPTED MANUSCRIPT

Downloaded from academic.oup.com/jxb/advance-article/doi/10.1093/jxb/erag557/9016158 by guest on 12 November 2026

[9] Plant Epigenomics, TUM School of Life Sciences, Technical University of Munich, Freising, Germany.

[10] Ecosystem Physiology, Faculty of Environment and Natural Resources, University Freiburg, Germany.

**Date of submission:** 29.7.2026

**Main figures:** 6

**Main tables:** 0

**Supplementary data:** Supplementary Fig. S1-S31; Supplementary Files S1-S28

**Word count (Introduction to start of Supplementary data, excluding Materials and methods):** 4971

# Highlight

S-nitrosoglutathione reductase deficiency was associated with altered transcriptomic responses following repeated climate stress and two generations of control growth, as well as changes in chromatin- and RNA-associated gene expression

# Abstract

Climate change exposes plants to recurrent and interacting stresses, yet the extent to which these effects persist across generations, and the mechanisms involved, remain unclear. Here, we compared *Arabidopsis thaliana* wild type (WT, Col-0) plants with *gsnor1-3* (hereafter, *gsnor-ko*), a mutant deficient in S-nitrosoglutathione reductase (GSNOR), an enzyme involved in nitric oxide homeostasis. Plants were propagated for three successive generations (G1-G3) under control, drought, elevated $CO_2$, $O_3$, heat (warm temperature), and combined treatment scenarios, followed by two recovery generations under control conditions (G4-G5). We quantified rosette growth, photosynthetic traits, seed production, and transcriptome dynamics by RNA-seq. Across environments, *gsnor-ko* exhibited reduced vegetative growth and reproductive output compared with WT. Transcriptomic responses were strongly scenario- and generation-dependent, with the

ACCEPTED MANUSCRIPT

Downloaded from academic.oup.com/jxb/advance-article/doi/10.1093/jxb/erag557/9016158 by guest on 12 November 2026

largest differential expression shifts observed under heat and combined-treatment (combination) conditions. Compared with WT, *gsnor-ko* showed greater transcriptome similarity across generations and among genes differentially expressed in response to the same treatment. Functional enrichment and candidate-gene analyses identified pathways/components linked to DNA methylation, heterochromatin maintenance, histone ubiquitination, $m^6A$ RNA regulation, and methyl-donor metabolism. Together, these findings are consistent with a model in which GSNOR activity contributes to transcriptomic recovery after repeated climate stress, whereas GSNOR deficiency is associated with recurrent or reconfigured stress-associated transcriptional states at G1, G3, and G5, suggesting epigenetically associated regulatory reconfiguration.

## Keywords

*Arabidopsis thaliana*; climate change; epigenetic regulation; GSNOR; nitric oxide; stress memory; transcriptomic resetting; multigenerational effects

## Abbreviations

$CO_2$, carbon dioxide

DAPC, discriminant analysis of principal components

DEG, differentially expressed gene

GLM, generalized linear model

*gsnor1-3*, *gsnor-ko*

GSNO, S-nitrosoglutathione

GSNOR, S-nitrosoglutathione reductase

$m^6A$, $N^6$-methyladenosine

NO, nitric oxide

NPQ_Lss, steady-state non-photochemical quenching

$O_3$, ozone

ACCEPTED MANUSCRIPT

Downloaded from academic.oup.com/jxb/advance-article/doi/10.1093/jxb/erag557/9016158 by guest on 12 November 2026

PPFD, photosynthetic photon flux density

PCA, principal component analysis

PSII, photosystem II

QYmax, maximum quantum yield

RdDM, RNA-directed DNA methylation

RNA-seq, RNA sequencing

VST, variance-stabilising transformation

WGCNA, weighted gene co-expression network analysis

# Introduction

Climate change is reshaping the plant environment through simultaneous shifts in temperature, water availability, and atmospheric composition (IPCC, 2023a). In addition to warming and drought, plants are increasingly exposed to rising concentrations of carbon dioxide ($CO_2$) and tropospheric ozone ($O_3$), which can often occur together rather than as isolated stresses (IPCC, 2023b). Because multiple stressors can trigger non-additive physiological and molecular responses, understanding plant adaptation under future climates requires experimental frameworks that integrate multiple environmental drivers across time (De Kauwe *et al.*, 2021; Montes *et al.*, 2022; Pascual *et al.*, 2022).

Plants can retain information from prior stress exposure, leading to physiological, transcriptional, or developmental stress memory that shapes subsequent responses (Zheng *et al.*, 2024). However, the stability and mechanism of this memory vary widely, and a critical distinction must be made between short-term somatic memory, intergenerational effects, and transgenerational inheritance. Foundational Arabidopsis studies reported stress-associated transgenerational effects under distinct conditions (Molinier *et al.*, 2006; Boyko *et al.*, 2010), whereas subsequent work also showed that stable, heritable methylome changes are not a general outcome of repeated drought stress (Ganguly *et al.*, 2017). Current evidence therefore strongly supports stress memory and priming in plants, but whether stress-induced states are stably transmitted through meiosis remains

ACCEPTED MANUSCRIPT

Downloaded from academic.oup.com/jxb/advance-article/doi/10.1093/jxb/erag557/9016158 by guest on 12 November 2026

context-dependent and is often unresolved (Crisp *et al.*, 2016; Erdmann and Picard, 2020; Pratx *et al.*, 2024). Broadening this perspective, work in poplar under future-climate-relevant drought-heat scenarios showed that transcriptomic responses were similar during stress but diverged strongly after recovery, supporting the concept of stress-related molecular memory and altered post-stress steady states in a climate-change context (Georgii *et al.*, 2019).

Epigenetic regulation provides a plausible molecular framework for the maintenance or resetting of stress-responsive states. DNA methylation, histone modifications, and histone variants can influence chromatin organisation and gene expression, while RNA modifications, such as $N^6$-methyladenosine ($m^6A$), provide an additional post-transcriptional regulatory layer (Reichel *et al.*, 2019; Liu and Lang, 2020; Ueda and Seki, 2020; Nunez-Vazquez *et al.*, 2022). Together, these systems are well-positioned to link environmental sensing to sustained changes in gene expression. Heat-stress memory, for example, is associated with prolonged transcription of memory-associated genes including APX2, HSP18.2, HSP21, HSP22, and HSA32 and chromatin-based maintenance mechanisms such as HSFA2/HSFA3-mediated H3K4 hypermethylation, while dehydration and osmotic stress can also involve DNA methylation changes and histone-associated regulation (Brzezinka *et al.*, 2016; Liu *et al.*, 2018; Korotko *et al.*, 2021; Friedrich *et al.*, 2021; Pratx *et al.*, 2023; Nishio *et al.*, 2024; Rao *et al.*, 2024; Behl *et al.*, 2026). These findings suggest that stress can leave a regulatory imprint beyond the initial exposure, although its maintenance or resetting remains context-dependent (Oberkofler *et al.*, 2021; Staacke *et al.*, 2025).

A hallmark of plant stress responses is the rapid production and signalling of reactive oxygen and nitrogen species (ROS and RNS, respectively) (Delledonne *et al.*, 1998; Durner *et al.*, 1998; Miller *et al.*, 2009). Nitric oxide (NO), a pivotal RNS, has emerged as a modulator of the transcriptome and epigenetic landscape (Skelly *et al.*, 2016; Lindermayr *et al.*, 2020). NO mainly signals through protein *S*-nitrosation (protein-SNO), a post-translational modification that targets regulatory thiol groups in proteins. *S*-nitrosation of the master immune transcriptional co-activator NONEXPRESSOR OF PATHOGENESIS-RELATED GENES 1 (NPR1) regulates its subcellular localisation and interactions with transcription factors, thereby driving the expression of thousands of defence-related genes (Tada *et al.*, 2008; Lindermayr *et al.*, 2010). Conversely, nucleosome repositioning mediated by the chromatin remodelling ATPase EMBRYO SAC DEVELOPMENT ARREST 16 (EDA16) dampens immune responses by selectively repressing a transcriptional

ACCEPTED MANUSCRIPT

Downloaded from academic.oup.com/jxb/advance-article/doi/10.1093/jxb/erag557/9016158 by guest on 12 November 2026

programme involved in the biosynthesis of the major cellular antioxidant glutathione (GSH) (Pardal *et al.*, 2021). GSH may react with NO to form the potent *trans*-nitrosylating agent, *S*-nitrosoglutathione (GSNO). Cellular GSNO pool is largely controlled by the evolutionarily conserved GSNO reductase 1 (GSNOR1) via the NADH-dependent reduction of GSNO to oxidised GSH and ammonium. GSNOR1-deficient *Arabidopsis* (*gsnor1-3,* hereafter *gsnor-ko*) plants exhibit overaccumulation of protein-SNO, resulting in reduced growth, delayed development, sensitivity to higher temperature and biotic stress, as well as tolerance to oxidative stress (Jensen *et al.*, 1998; Liu *et al.*, 2001; Feechan *et al.*, 2005; Lee *et al.*, 2008; Chen *et al.*, 2009; Holzmeister *et al.*, 2011). Our previous work demonstrated that *gsnor-ko* exhibits altered chromatin accessibility and, therefore, transcription of stress-responsive genes. Mechanistically, this epigenetic reprogramming is underpinned by the accumulation of the primary methyl donor for DNA and histone methylation, S-adenosylmethionine, and the inhibitory *S*-nitrosation of the histone modifier, HISTONE DEACETYLASE 6 (HDA6) (Ageeva-Kieferle et al., 2021; Rudolf et al., 2021; Lindermayr et al., 2010). It remains unknown, however, if GSNOR1 drives stress-specific transcriptional programmes across generations and affects subsequent transcriptional recovery.

Here, we used a five-generation Arabidopsis experiment to test how repeated exposure to future-climate scenarios shapes phenotypic and transcriptomic responses in wild type and the nitric oxide homeostasis mutant *gsnor-ko*. Specifically, we tested three interconnected hypotheses: 1. In addition to immediate phenotypic and transcriptional responses, repeated future-climate scenarios produce multigenerational carryover effects. 2. GSNOR activity contributes to post-stress transcriptional recovery. 3. Differences in transcriptional recovery between wild-type and *gsnor-ko* plants reflect altered regulatory resetting rather than only stress severity. In this framework, we therefore examine whether NO/redox homeostasis is associated with recovery or continued detection of stress-responsive states, while treating chromatin- and RNA-linked pathways as candidate contributors.

ACCEPTED MANUSCRIPT

Downloaded from academic.oup.com/jxb/advance-article/doi/10.1093/jxb/erag557/9016158 by guest on 12 November 2026

# Materials and methods

## 1. Plant material and cultivation

Seeds of *A. thaliana* ecotype Col-0 (WT) were obtained from the Nottingham Arabidopsis Stock Centre (NASC). The *gsnor1-3* mutant line (also reported as *hot5-2*; GABI-Kat line 315D11) was obtained from GABI-Kat (Rudolf *et al.*, 2021). Both WT and *gsnor-ko* plants were grown in soil (Floradur® Anzucht Substrat, Floragard, Germany; substrate 0.5 kg/m3 NPK fertiliser (18-10-20) and trace elements) mixed with quartz sand (0.6 to 1.2mm) (4:1) in individual standard Photon Systems Instruments (Photon Systems Instruments-PSI Brno, Czechia) pots (6cm × 6cm × 9.5cm), containing 170g soil mix. These pots were placed in trays (5 × 4 pots per tray) and registered into the PSI PlantScreen™ system. After stratification for 2–3 d at 4°C in darkness, pots were transferred to the ExpoSCREEN chambers and cultivated under long-day conditions (14 h light / 10 h dark) at a photosynthetic photon flux density (PPFD) of 300 µmol $m^{-2}$ $s^{-1}$. Leaf tissue was harvested from 4- to 5-week-old rosettes at 3 h (from 9:00 to 10:00) after lights-on, flash-frozen in liquid nitrogen, and stored at −70 °C until extraction.

## 2. Multi-generational experimental design

### 2.1 Overview and generation scheme

Plants were propagated in a multi-generational experiment as described in Fig. 1A and Supplementary Fig. S1A. Seeds from one WT and one *gsnor-ko* G0 plant were used to establish G1 (approximately 3 months for each generation). Within each genotype and treatment, four G1 plants were selected as progenitors for G2. Each progenitor produced a separate offspring family, from which approximately ten plants were grown, giving approximately 40 plants per genotype × treatment in G2. Four progenitor plants were again selected within each treatment lineage to establish the subsequent generation, and this propagation scheme was continued through G5. We refer to descendants of a selected progenitor within a treatment as a pedigree. Plants sampled from the same pedigree may therefore share a parent or ancestor and are not wholly independent observations.

For phenotyping, 10 plants were sampled per genotype × treatment × generation group. From G2 onward, these were drawn from the four pedigree families (three, three, two, and two plants per family). For RNA-seq, four plants were sampled per genotype × treatment group in each of the analysed generations (G1, G3,

ACCEPTED MANUSCRIPT

Downloaded from academic.oup.com/jxb/advance-article/doi/10.1093/jxb/erag557/9016158 by guest on 12 November 2026

and G5). Control groups comprised five plants, except for the WT control in G1, which comprised six. In G3 and G5, the four treatment libraries generally represented one plant from each of four recorded pedigrees; the five control libraries represented four recorded pedigrees, with two plants from one pedigree as described in Supplementary File S24. To minimise positional effects, pots were redistributed within chambers every 10-12 days using a random placement scheme. The six environmental scenarios were imposed concurrently in designated subchambers within two large climate chambers. Each scenario occupied one fixed subchamber per generation, without independent chamber replication or rotation of treatment assignments. Generations were grown sequentially as a connected propagation experiment and therefore do not constitute independent repetitions of the experiment.

## 2.2 Climate scenarios/treatments

Temperature regimes were designed to mimic naturally occurring local seasonal conditions for the Munich region, based on per-minute 2 m air-temperature records monitored at the Deutscher Wetterdienst (DWD) station München-Flughafen (station ID 01262; 48°22′ N, 11°48′ E; 453 m a.s.l.), downloaded from the DWD Climate Data Centre archive (Supplementary File S1) (Deutscher Wetterdienst, 2026). For control conditions, a slightly modified per-minute temperature profile derived from June to August 1993 was implemented (monthly mean temperatures: 16.5°C, 16.1°C, and 17.1°C, respectively). For the heat simulation, per-minute temperature profiles derived from June–August 2003 were used (monthly mean temperatures: 21.5°C, 20.4°C, and 22.4°C, respectively), reflecting a historically hot summer and intended to approximate conditions projected to become typical near the end of the century, roughly the 2080s, under high-emissions scenarios in Bavaria (Bayerisches Staatsministerium für Umwelt und Verbraucherschutz, 2021) (Fig. 1B; Supplementary File S1). To avoid confounding effects from the temperature treatment, the temperature during a few days in the 1993 climate program was consistently lower than in the 2003 program throughout the climate simulation. The final mean temperature differences between the heat and control programs were approximately +5.0°C (June), +4.3°C (July), and +5.3°C (August) across the temperature regimes (Fig. 1B; Supplementary Fig. S2A).

Under control conditions of the 1993 simulation scenario, atmospheric $CO_2$ concentrations were 400/400 ppm (day/night), and $O_3$ was ~5/5 ppbv (day/night; also negligible, as it was scrubbed by charcoal filters in the chambers) and plants were well-watered. Future climate scenarios included enhanced $CO_2$ levels of 550 ppm (day/night), a concentration projected to be reached by

ACCEPTED MANUSCRIPT

Downloaded from academic.oup.com/jxb/advance-article/doi/10.1093/jxb/erag557/9016158 by guest on 12 November 2026

approximately 2050 under SSP5-8.5 and by 2070 under SSP2-4.5, depending on the climate scenario (Meinshausen *et al*., 2020). Plants were exposed to 100 ppb $O_3$ during the day and 50 ppb $O_3$ at night to mimic an elevated summer urban/peri-urban ozone regime rather than background conditions (Fitzky *et al.*, 2019; Im *et al.*, 2013). Drought stress was applied by reducing soil water content to approximately 50% of the control value (Fig. 1; Supplementary Fig. S2 and S3; Supplementary Files S3-S5). Except for drought, treatments were initiated 1 week after germination; drought was imposed from the start (see Section 3.2).

# 3. Climate chamber settings and environmental monitoring

## 3.1 Baseline growth conditions

Simulation of the different environmental conditions was performed using the ExpoSCREEN facility at Helmholtz Munich (HMGU), as previously described (Vanzo *et al.*, 2015; Ghirardo *et al.*, 2020; Roy *et al.*, 2021). The experimental setup consisted of two large climate chambers, each subdivided into separately equipped subchambers. Temperature was regulated at the level of the main climate chamber, whereas atmospheric $CO_2$ and $O_3$ concentrations and watering regimes could be adjusted for individual subchambers.

One main chamber was operated under the elevated-temperature regime and accommodated the heat and combination treatments in separate subchambers. In the combination treatment, elevated temperature was combined with increased $CO_2$ and $O_3$ concentrations and an adjusted watering regime (see Section 3.2). The second main chamber was operated under the control-temperature regime and accommodated the control, elevated $CO_2$, elevated $O_3$, and drought treatments, each in a designated subchamber.

Each environmental treatment was assigned to a single subchamber per generation, and these assignments remained unchanged throughout the five-generation experiment because reconfiguration of the gas-delivery systems and associated sensors was not technically feasible. Consequently, environmental treatments were not independently replicated across chambers or subchambers. Within each treatment subchamber, wild-type (WT) and *gsnor-ko* plants were cultivated together under the same environmental conditions.

ACCEPTED MANUSCRIPT

Downloaded from academic.oup.com/jxb/advance-article/doi/10.1093/jxb/erag557/9016158 by guest on 12 November 2026

Each subchamber is made of acrylic glass (about 1 $m^3$ in volume) and was equipped with combined air temperature and relative humidity sensors (ifm, Switzerland) and was flushed (80 $m^3$ $h^{-1}$) with purified air (charcoal-filtered) to adjust temperature and humidity for each ExpoSCREEN chamber, providing the same temperature and humidity in all subchambers of the respective 'large' chamber. To achieve irradiation regimes very close to outdoor solar conditions, from UV to near-infrared, the phytotron facility used a combination of lamps and filters that simulate the daily course of solar radiation from sunrise to sunset (Thiel *et al.*, 1996). Details about climate conditions in subchambers are reported in the Supplementary Files S2-S7. Plants were watered manually by adding water directly to the trays. Watering decisions were based on pot weight and chamber conditions (temperature program) (Supplementary Files S2, S6, and S7). PPFD was set to 300 µmol $m^{-2}$ $s^{-1}$ at plant height (Supplementary File S4). Plants were fertilised with Compo Complete Pflanzendünger (liquid fertiliser, Brand Compo, EAN 4008398135737, 3ml dissolved in 1 litre of water) at the end of weeks 3 and 4. Due to technical issues with the chamber sensors, temperature, humidity, and fumigation data were not recorded for 13 days for G1 (control, $CO_2$, drought, and $O_3$) and for 3 days for G4 (Supplementary Fig. S2 and S3; Supplementary Files S2-S5).

### 3.2 Drought treatment

Drought was imposed from the start of the experiment by allowing water to evaporate from pre-watered pots until they reached a weight of 220 g (pot + soil + water), corresponding to an estimated Soil Water Content (SWC, vol-%) of approximately 23%vol. SWC was measured using a soil moisture meter (HH2) connected to a ThetaProbe (ML2x; Delta-T Devices, Britain, UK). After sowing, drought pots were watered ~45–50% less than control plants. Heat-treated plants were watered ~45-50% more than control plants, and combination-treated plants were watered ~50% less than heat-treated plants and, in some cases, were similar to controls, as combination plants also experienced heat treatment. This was done to compensate for the higher VPD and evaporative demand under heat and to prevent plants from lethal drying (Supplementary Fig. S3 and Supplementary Files S6-S7).

## 4. Experimental timeline, sampling strategy and statistical analysis

Plants were phenotyped using a PSI PlantScreen™ platform (Photosystem Instruments Brno, Czechia) at the end of week 3 and week 4, including morphological traits (e.g., rosette area) and

ACCEPTED MANUSCRIPT

Downloaded from academic.oup.com/jxb/advance-article/doi/10.1093/jxb/erag557/9016158 by guest on 12 November 2026

chlorophyll fluorescence parameters (e.g., Maximum Quantum Yield of Photosystem II - QYmax and Non-Photochemical Quenching - NPQ_Lss). QYmax (Fv/Fm) was used as an estimate of the maximum efficiency of Photosystem II (PSII) photochemistry in dark-adapted tissue, whereas NPQ_Lss was used as a measure of non-photochemical quenching at light steady phase and photoprotective heat dissipation during illumination (Baker, 2008; Murchie and Lawson, 2013).

Exported PSI data were analysed in R (using packages car, emmeans, multcomp, and tidyverse) (Supplementary Files S8-S12). Phenotypic traits were analysed using Generalised Linear Models (GLM) with a Gaussian error distribution. For the week 3 and week 4 PSI measurements, genotype, treatment, and generation were included as fixed factors, along with their interactions. Overall model effects were evaluated by Type III analysis of variance, and estimated marginal means were calculated for post hoc comparisons. Pairwise contrasts were used to compare genotypes within treatment × generation combinations and treatments within genotype × generation combinations, with p-values adjusted by the Benjamini–Hochberg method. For treatment-specific plots, separate Gaussian GLMs were fitted within each treatment using genotype, generation, and their interaction as predictors, followed by Tukey-adjusted post hoc tests and compact letter displays. Descriptive statistics are reported as mean ± SE. No additional dark-adaptation time was needed for the fluorescence measurements in the PSI system, as plants were transferred to the PSI platform the evening before measurement and measured the next morning, before lights-on. However, due to an error in the PSI software, plant trays in G3 (all treatments at week 3) and G4 (all treatments at week 4) were re-measured after a 30-minute dark-adaptation period. Since the error at the facility took some time for the PSI company to repair, we could not measure the fluorescence parameters of G4. Because the additional dark-adaptation and remeasurement procedure was applied to all G3 week 3 trays and to the G4 week 4 trays, comparisons involving these groups may include a procedural effect. To assess sensitivity to remeasurement, original and repeat observations were matched by plant ID. Within each genotype, treatment-minus-control contrasts were calculated at both occasions, and differences in their changes were tested; results are provided in Supplementary File S27.

Individual plants provided biological observations within each genotype × treatment × generation group. However, each environmental treatment was applied to a single, fixed subchamber within a generation. Each treatment had one environmental unit per generation. Individual plants were sampled within that unit,

ACCEPTED MANUSCRIPT

Downloaded from academic.oup.com/jxb/advance-article/doi/10.1093/jxb/erag557/9016158 by guest on 12 November 2026

but no replicate environmental units were available for estimating treatment effects independently of chamber or subchamber effects. Temperature was controlled at the large-chamber level, so the heat and combination subchambers did not constitute independent replicates of the temperature regime. Statistical comparisons among treatments describe differences observed under the assigned chamber conditions. WT–*gsnor-ko* comparisons within a treatment were made between plants co-grown in the same subchamber. The reported phenotypic models included genotype, treatment, and generation as fixed factors and treated measurements from individual plants as observations; pedigree and immediate-parent identity were not included as model terms. The RNA-seq differential-expression analyses likewise did not include a pedigree or parent-identity term.

For sequencing, two random fully elongated (mature) leaves per individual plant were harvested at week 4.5 (3 h after lights-on; 9:00-10:00). Leaves for RNA-seq were harvested individually for each plant and not pooled. Seeds from each plant were collected and weighed to quantify reproductive output across treatments. They were harvested at approximately week 10 (WT) and week 11 (*gsnor-ko*), corresponding to comparable reproductive/developmental stages rather than identical chronological ages, as the mutant generally developed more slowly than WT. At harvest, siliques had turned brown/dry, and seeds were fully matured. Seeds were collected per individual plant (and were not pooled) and stored at 4°C (Supplementary Fig. S1A; Supplementary File S10). Additionally, seed phenotyping was performed using the phenoSeeder platform to complement seed weight measurements (Jahnke *et al.*, 2016; Klasen *et al.*, 2025). Individual seed mass was measured using phenoSeeder in WT at G1, G3, and G5, with three technical replicates per generation × scenario combination. Individual-seed measurements were averaged within each technical repetition. These means were analysed separately within each scenario using a GLM with generation as the explanatory factor, followed by Tukey-adjusted comparisons of estimated marginal means. Because the repetitions were technical rather than independent biological replicates, these comparisons describe differences among the measured seed samples and do not establish population-level biological differences. Individual seeds were treated as subsamples. Total seed yield per plant was analysed separately within each treatment using a Gaussian GLM with genotype, generation and their interaction. Individual-seed mass was analysed only in WT using the technical-repetition means and generation-only models (as for PSI data).

ACCEPTED MANUSCRIPT

Downloaded from academic.oup.com/jxb/advance-article/doi/10.1093/jxb/erag557/9016158 by guest on 12 November 2026

# 5. RNA extraction, library preparation, sequencing and transcriptome analysis

## 5.1 RNA extraction, library preparation, and sequencing

RNA-seq was performed using snap-frozen leaf tissue collected individually from plants in generations G1, G3, and G5. Two fully elongated leaves were sampled per plant without pooling tissue between plants. Total RNA was extracted from approximately 50 mg of ground tissue using an in-house protocol based on the Sigma TRI Reagent method (Chomczynski and Sacchi, 1987). RNA quantity and integrity were assessed using a NanoDrop spectrophotometer and a Bioanalyzer, respectively.

Sequencing libraries were prepared by BMK Gene GmbH (Münster, Germany) using poly(A)-enriched RNA and sequenced on a DNBSEQ-T7 platform as 150 bp paired-end reads, generating approximately 9 GB per sample, corresponding to approximately 30 million reads per sample.

## 5.2 Read preprocessing, alignment, quantification, and quality assessment

Primary read quality assessment, adapter removal, and quality trimming were performed by BMK Gene GmbH. Processed reads were aligned to the *Arabidopsis thaliana* TAIR10 reference genome using HISAT2 version 2.2.1. Approximately 97% of reads mapped to the reference genome. Sequencing quality was assessed across libraries using quality-score summaries and representative per-base quality profiles (Supplementary Fig. S4A–B).

Read counts were generated using featureCounts version 2.0.2 with the parameters -T 12 -p -t exon -g Parent --primary (Liao et al., 2013). The TAIR10 GFF3 annotation file, accessed on 19 June 2023, was converted to GTF format in R before quantification. The RNA-seq computational workflow is summarised in Supplementary Fig. S1B.

Sample relationships and replicate consistency were assessed by hierarchical clustering of variance-stabilised expression values (Supplementary Fig. S5). Libraries were sequenced in separate batches, including a second batch of WT G1 libraries and sequencing was performed at different times for the sampled generations. Documented batch effects were accounted for in differential-expression models where applicable, as described in Section 5.4.

ACCEPTED MANUSCRIPT

Downloaded from academic.oup.com/jxb/advance-article/doi/10.1093/jxb/erag557/9016158 by guest on 12 November 2026

## 5.3 Multivariate transcriptome analyses

Count data were transformed using the variance-stabilising transformation implemented in DESeq2 version 1.42.1 before multivariate analysis. Discriminant analysis of principal components (DAPC) was performed separately for WT and *gsnor-ko*, with treatment × generation combinations used as predefined classes. Classification performance was evaluated using cross-validation and confusion matrices, which summarised the classification frequencies for each class (Fig. 3A; Supplementary Fig. S6A–B).

Principal component analysis (PCA) was performed on variance-stabilised expression values to assess the unsupervised structure of the transcriptome and sample overlap. PCA plots were examined alongside hierarchical clustering and DAPC to evaluate relationships among treatments and sampled generations. The percentages of variance explained by PC1 and PC2 are indicated on the corresponding PCA axes (Supplementary Fig. S6C–D). These complementary analyses were used to assess the consistency of sample grouping and the extent of overlap among experimental classes.

## 5.4 Differential expression and interaction analyses

Differential expression analysis was performed using DESeq2 version 1.42.1. Within each genotype and sampled generation, each treatment was compared with the corresponding control from the same generation. The design formula was ~ treatment for datasets without a documented batch effect and ~ batch + treatment when adjustment for sequencing batch was required. Genes with a Benjamini–Hochberg-adjusted *P*-value < 0.05 were considered differentially expressed. No minimum absolute $\log_2$ fold-change threshold was applied in the primary analysis. As sensitivity analyses, DEG counts, and trajectory classifications were recalculated after applying post hoc absolute $\log_2$ fold-change cutoffs of 0.2 and 0.5. These filters were applied to estimated effects after differential-expression testing and did not constitute formal tests against a nonzero effect-size threshold.

To test whether treatment-associated expression differed between genotypes, additional DESeq2 models were fitted separately for G1, G3, and G5. The G1 design was ~ WT_G1_batch2 + genotype * treatment, where WT_G1_batch2 identified the documented second batch of WT G1 libraries. The design was ~ genotype * treatment for G3 and G5. For each treatment, the genotype

ACCEPTED MANUSCRIPT

Downloaded from academic.oup.com/jxb/advance-article/doi/10.1093/jxb/erag557/9016158 by guest on 12 November 2026

× treatment coefficient tested the difference between the treatment-versus-control $\log_2$ fold changes in *gsnor-ko* and WT. Genes were considered to have a significant interaction when the Benjamini–Hochberg-adjusted *P*-value was < 0.05. The number of significant interactions and genes with testable adjusted *P*-values is reported in Supplementary File S25.

At G5, treatment labels refer to treatment history because all plants were grown under control conditions during G4 and G5. Consequently, G5 comparisons assess expression differences associated with previous treatment exposure relative to the corresponding control lineage. Pedigree and immediate-parent identity were not included as model terms, as described in Section 4. Calculations and visualisations were performed in R and RStudio, with figure adjustments performed in Inkscape.

## 5.5 DEG overlap and trajectory analyses

Three-generation DEG overlap was evaluated separately for each genotype and treatment using treatment-versus-control comparisons from G1, G3, and G5. Genes with non-missing adjusted *P*-values and $\log_2$ fold changes were considered eligible in each generation. The observed three-way intersection was expressed as a percentage of the DEG set size for each sampled generation.

To assess whether the observed overlap exceeded chance expectations, 20,000 random sets matching the observed DEG-set sizes were generated. Sets were drawn independently for each generation from that generation's eligible genes. The observed three-way intersection was compared with the resulting null distribution using a one-sided permutation test. *P*-values were adjusted across the ten genotype × treatment comparisons using the Benjamini–Hochberg method. DEG-set sizes, overlap proportions, expected overlaps, and permutation-test results are reported in Supplementary File S23.

For trajectory analysis, genes were assigned an expression state at each sampled generation relative to the corresponding genotype- and generation-matched control: upregulated when adjusted $P < 0.05$ and $\log_2$ fold change > 0; downregulated when adjusted $P < 0.05$ and $\log_2$ fold change < 0; and no significant differential-expression state when adjusted $P \geq 0.05$ or no significant result was available. An unavailable result was not interpreted as evidence of unchanged expression. State transitions across G1, G3, and G5 were visualised using alluvial plots (Supplementary Fig. S18).

ACCEPTED MANUSCRIPT

Downloaded from academic.oup.com/jxb/advance-article/doi/10.1093/jxb/erag557/9016158 by guest on 12 November 2026

In the three-point trajectory analysis, persistent genes were defined as genes significantly differentially expressed in the same direction at G1, G3, and G5. Switcher genes showed a reversal between significant upregulation and downregulation across sampled generations. Fading trajectories described earlier differential-expression states that were no longer detected at G5, whereas emergent trajectories described states first detected at a later sampling point.

For individual-gene heatmaps, the original selection rules also permitted two-point same-direction patterns for WT $CO_2$, WT $O_3$, and *gsnor-ko* drought; the *gsnor-ko* drought rule additionally required the absence of a significant G5 state. These patterns were distinguished from recurrence across all three sampled generations (Supplementary Figs. S19–S22). Neither designation establishes uninterrupted differential expression during the unsampled G2 and G4 generations.

The sensitivity of DEG counts and trajectory assignments was assessed by applying post hoc absolute $\log_2$ fold-change cutoffs of 0.2 and 0.5 to genes meeting the adjusted *P*-value threshold and repeating the applicable classification rules. DEG-count sensitivity and persistent/switcher classification sensitivity are reported in Supplementary Files S26 and S28, respectively.

## 5.6 Weighted gene co-expression network analysis (WGCNA)

WGCNA was performed using variance-stabilised expression values. An unsigned network was constructed using a soft-thresholding power of 11, a minimum module size of 40, and deepSplit = 2. Module eigengenes were calculated, and their relationships with experimental groups were evaluated using Pearson correlations. Functional annotation of selected modules was performed using Mercator (Langfelder et al., 2008; Langfelder and Horvath, 2008; Yip and Horvath, 2007). Network construction and module relationships are presented in Supplementary Figs. S24–S29.

## 5.7 Assessment of circadian sampling consistency

To assess whether variation in sampling time could contribute to transcriptome differences, expression patterns of established morning- and evening-phased circadian marker genes were examined in WT and *gsnor-ko* across control, drought, elevated $CO_2$, elevated $O_3$, heat, and combination groups in G1, G3, and G5. At G5, these groups represented treatment histories rather than ongoing exposures.

ACCEPTED MANUSCRIPT

Downloaded from academic.oup.com/jxb/advance-article/doi/10.1093/jxb/erag557/9016158 by guest on 12 November 2026

Variance-stabilised expression values were used for PCA and comparisons of morning- and evening-phased marker expression across experimental groups (Supplementary Fig. S7A–B). Normalised expression profiles of representative marker genes were also examined in control samples across generations (Supplementary Fig. S7C). Treatment-associated $\log_2$ fold changes relative to the corresponding genotype- and generation-matched controls were assessed separately (Supplementary Fig. S7D). Control marker-gene profiles were broadly comparable across generations, supporting sampling consistency at the resolution of this analysis.

## 6. Functional enrichment analysis and Candidate gene selection

Functional enrichment analysis was performed separately for up- and down-regulated genes in each genotype × generation × treatment comparison. Genes were classified as differentially expressed with an adjusted p-value < 0.05; the sign of the $\log_2$ fold change indicated the direction. Gene sets were annotated using Mercator categories at levels 1–8 and analysed with clusterProfiler's enricher function. For each comparison, the background comprised genes with non-missing adjusted p-values and $\log_2$ fold changes in their DESeq2 results that also matched the Mercator annotation at the level being tested. Mercator terms containing 10–500 background genes were tested. Enrichment p-values were adjusted using the Benjamini–Hochberg method; the analysis used a p-value cutoff of 0.05 and a q-value cutoff of 0.20.

Candidate genes for Figs 5–6 were identified by examining genes associated with the enriched chromatin- and RNA-related functional categories and assessing their reported functions in the literature. Candidates were assigned to five literature-informed regulatory models according to those functions; assignments were not derived from statistical clustering or from a required expression trajectory. Genes could belong to more than one model, as supported by the literature. Expression patterns were assessed for individual genes across the indicated contrasts. Enrichment statistics apply to the tested functional categories, and differential expression statistics apply to individual genes; no separate statistical significance test was performed for the five models collectively. Gene functions and supporting references are documented in Supplementary File S21.

**7. Pathogen infection**

For disease assays, plants were grown in soil in a controlled-environment chamber at 21°C, 100 $\mu mol\ m^{-2}\ s^{-1}$ light, 50-65% relative humidity, and a photoperiod of 16/8 h light/dark. *Pseudomonas*

ACCEPTED MANUSCRIPT

Downloaded from academic.oup.com/jxb/advance-article/doi/10.1093/jxb/erag557/9016158 by guest on 12 November 2026

*syringae* pv. maculicola (Psm) ES4326 were cultivated overnight in LB medium containing 10 mM $MgSO_4$ and kanamycin (50µg/mL) at 28°C, harvested by centrifugation and resuspended to $OD_{600}$ = 0.0005 in 10 mM $MgSO_4$. Leaves of comparable age and size were infiltrated with the bacterial suspension on the abaxial surface using a 1 mL syringe. For each experimental condition, 16–18 leaves were infiltrated (≤2 per plant), and plants were maintained in the growth chambers for 5 days after inoculation. Leaf extracts were serially diluted in 10 mM $MgSO_4$ and streaked in parallel on LB agar supplemented with kanamycin. After incubation at 28°C for 2 days, colonies were counted and bacterial titre calculated per leaf disc (Frungillo *et al.*, 2023, Preprint).

The 16–18 infiltrated leaves per condition represent leaf measurements, with no more than two leaves sampled per plant. Plant identifiers were not retained with the leaf-level measurements, so the exact number of independent plants per condition and within-plant correlation cannot be reconstructed. The pathogen data are therefore presented as exploratory leaf-level observations rather than independent plant-level replicates.

**8. AI usage in Data analysis**

For data analysis, an AI tool (ChatGPT 5.4) was used for programming in R (2024.12.1+563). After using this tool/service, the author(s) reviewed and edited the codes as needed and take(s) full responsibility for the content of the published article.

# Results

*Arabidopsis thaliana* WT and the NO-homeostasis mutant *gsnor-ko* were propagated for five successive generations in controlled-climate chambers under current and projected future climate scenarios (Fig. 1; Supplementary Fig. S1A; see Materials and Methods).

## 1. Phenotypic responses to climate scenarios are genotype and generation specific

### 1.1 Rosette growth responses are stress- and generation-dependent

Rosette area varied with climate scenario and generation, with the largest WT rosettes observed under heat in G2 (Fig. 2A–B). Across environments, *gsnor-ko* plants were smaller than WT. This

ACCEPTED MANUSCRIPT

Downloaded from academic.oup.com/jxb/advance-article/doi/10.1093/jxb/erag557/9016158 by guest on 12 November 2026

difference was particularly pronounced under heat in G2, when the mean rosette area was 4842.5 mm² in WT and 1599.6 mm² in *gsnor-ko* (adjusted $p < 0.001$). Differences between genotypes were also evident in G5 after stress withdrawal (Supplementary Files S12–S13). Because *gsnor-ko* rosettes were smaller than WT rosettes even under control conditions, we also evaluated rosette area relative to the corresponding control within each genotype and generation (Supplementary Fig. S8). The normalised responses varied with treatment history and generation; then we interpreted them alongside, rather than replaced by, the absolute-area measurements. The week 3 measurements showed a similar overall difference in genotype (Supplementary Fig. S9; Supplementary Files S14–S15).

Rosette area also declined in G3 across several conditions, including the control, indicating a generation-wide component to the growth pattern (Fig. 2B). The extent of the decline and subsequent changes in G4–G5 varied by treatment and genotype. Thus, we interpreted treatment effects on plants grown relative to the corresponding control condition within each generation (Supplementary Fig. S8).

### 1.2 Photosynthetic performance is comparatively stable, with genotype- and generation-specific shifts

QYmax varied less across treatments and generations than rosette area, despite statistically significant effects of genotype, treatment and generation (Supplementary Fig. S10–S11; Supplementary Files S12–S15). Thus, the smaller rosettes of *gsnor-ko* were not accompanied by a decline in maximum PSII efficiency. NPQ_Lss showed greater condition- and generation-dependent variation, indicating changes in photoprotective energy dissipation (Supplementary Fig. S12–S13). In the paired remeasurement analysis (for G3 and G4), 30 of 34 available treatment-minus-control contrasts retained their direction. Four changed direction, and the G3 WT combination contrast for rosette area increased significantly between occasions (BH-adjusted $P = 0.0166$; Supplementary File S27). The two occasions, therefore, cannot be treated as fully interchangeable.

### 1.3 Reproductive output across climate scenarios in *gsnor-ko* and WT

Seed weight per plant was lower in *gsnor-ko* than in WT across treatments and generations, with mutant yields typically reaching approximately 7–27% of WT values (Supplementary Fig. S14A;



ACCEPTED MANUSCRIPT

Downloaded from academic.oup.com/jxb/advance-article/doi/10.1093/jxb/erag557/9016158 by guest on 12 November 2026

Supplementary File S16). WT seed production varied across generations and increased in G4–G5 after stress withdrawal, in lineages previously exposed to drought, heat or the combination treatment. In contrast, *gsnor-ko* seed production remained low, with no significant generation-to-generation contrasts within the mutant in this analysis (Supplementary Files S16–S17).

In WT, phenoSeeder measurements also showed changes in seed-trait distributions across generations, particularly following heat and combination treatments (Supplementary Fig. S14B–C; Supplementary Files S18–S19).

# 2. Pattern of differential expression across climate scenarios and generations

## 2.1 Wild type exhibits scenario- and generation-dependent DEG responses

Differential expression analysis revealed scenario- and generation-specific responses in WT (Fig. 3A–B). DEG numbers ranged from four under elevated $CO_2$ in G1 to 6,160 under the combination treatment in G1. Drought and combination lineages showed progressively fewer DEGs across the sampled generations. In contrast, the elevated-$CO_2$ response increased towards G5, whereas the number of heat-associated DEGs increased from G1 to G3 before declining at G5. The $O_3$ response was greatest in G3 (Fig. 3B; Supplementary Fig. S15A). These counts reflect the extent of detectable differential expression; individual gene trajectories are examined in Section 4.

## 2.2 DEGs in *gsnor-ko* show altered magnitude and directionality

In *gsnor-ko*, DEG numbers and the balance of up- and down-regulation also depended on scenario and generation (Fig. 3B; Supplementary Fig. S15B). Compared with WT, the mutant generally showed large DEG sets in $O_3$, heat, and their combination contrasts, although this pattern was not uniform across treatments or generations. Responses under drought, $CO_2$, and $O_3$ were highest in G3, whereas heat and combination responses decreased from G1 to G3 and increased again in G5. Across both genotypes, the DEG-count patterns were largely retained after applying a post hoc absolute $\log_2$ fold-change cutoff of 0.2 (Supplementary File S26).

The proportion of DEGs shared across G1, G3, and G5 varied by genotype and treatment (Fig. 3C; Supplementary Fig. S16A–B). In WT under heat, 55 genes were shared, representing 1.38%, 1.18%, and 21.83% of the G1, G3, and G5 DEG sets, respectively. This was approximately 2.50

ACCEPTED MANUSCRIPT

Downloaded from academic.oup.com/jxb/advance-article/doi/10.1093/jxb/erag557/9016158 by guest on 12 November 2026

times the overlap expected from the eligible gene sets (22.0 genes; BH-adjusted permutation p = $1.25 \times 10^{-4}$). In *gsnor-ko* under the combination treatment, 541 genes were shared, representing 7.96%, 31.79%, and 11.55% of the respective DEG sets, approximately 2.13 times the expected overlap (254.4 genes; BH-adjusted permutation p = $1.25 \times 10^{-4}$). Overall, seven of the ten genotype–treatment combinations showed three-generation overlap above chance expectations, although the proportions and enrichments varied among treatments (Supplementary File S23).

Because differences in DEG numbers do not directly test whether genotypes respond differently, we performed genotype × treatment interaction analyses within each sampled generation (Supplementary File S25). Significant interactions were detected for several treatments in G1 and G3, including combination (5,146 and 3,174 genes, respectively) and heat (4,659 and 3,185 genes, respectively). At G5, genotype-dependent treatment-history effects were detected most frequently for $CO_2$ (1,768 genes), followed by combination (237), $O_3$ (82), and drought (4). No G5 heat interaction met the adjusted p-value threshold. Thus, the genotype-dependent expression differences, as supported by formal interaction tests, varied across treatments and generations.

## 3. Functional analyses identify chromatin- and RNA-linked regulation as candidate layers of the multi-generational stress response

To interpret stress-responsive transcriptome changes, we performed functional enrichment analysis on up- and down-regulated gene sets for each treatment x generation x genotype combination and summarised the results using Mercator categories. To emphasise reproducible biology rather than isolated contrasts, we further grouped enriched terms into shared between genotypes and epigenetic-associated categories and visualised significant hits across the dataset (Fig. 4). Both genotypes showed recurrent enrichment of functions related to photosynthesis, redox regulation, nutrient uptake, RNA processing, and stress-associated transcription factors. These shared categories indicate that repeated climate exposure engaged overlapping metabolic and regulatory responses in WT and *gsnor-ko*.

Enriched categories also included histone and chromatin structure, RNA modification and transport, and ubiquitin-related functions (Fig. 4). These regulatory categories were generally broader in *gsnor-ko*, particularly under $O_3$, heat, and combination conditions (Supplementary Fig. S17–S18). Functional enrichment identifies pathways associated with differentially expressed



ACCEPTED MANUSCRIPT

Downloaded from academic.oup.com/jxb/advance-article/doi/10.1093/jxb/erag557/9016158 by guest on 12 November 2026

genes; it does not establish changes in chromatin marks or their inheritance. Taken together, the enrichment analyses indicate that multi-generational stress responses in this system involve not only metabolic and photosynthetic remodelling but also repeated engagement of chromatin-, histone-, RNA-, and redox-linked regulatory functions.

# 4. Recurrence and turnover of environmental factor-responsive genes across generations

## 4.1 Gene-state flow reveals fading, emergent, persistent, and switcher behaviour

To examine trajectories beyond DEG counts and overlap, we assigned each gene within a treatment to one of three states in G1, G3, and G5 relative to its corresponding control: up-regulated (adjusted $p < 0.05$ and $\log_2$ fold change $> 0$), down-regulated (adjusted $p < 0.05$ and $\log_2$ fold change $< 0$), or not differentially expressed (adjusted $p \geq 0.05$ or no significant result). No minimum absolute $\log_2$ fold-change threshold was applied. These states were used to construct the alluvial plots (Supplementary Fig. S18). In the three-point trajectory analysis, "persistent" denotes the same significant direction at G1, G3, and G5. For the individual-gene heatmaps and their sensitivity analysis, the original plotting rules also permitted two-point same-direction patterns for WT $CO_2$, WT ozone, and *gsnor-ko* drought; the *gsnor-ko* drought rule additionally required that no significant G5 state be present. These two-point patterns are identified separately and do not establish a response at all three sampled generations. Neither the three-point nor the two-point designation establishes uninterrupted differential expression in the unsampled G2 and G4 generations. We describe a response as fading when an earlier differential-expression state was no longer detected in G5, emergent when it was first detected at a later sampling point, and switching when its detected direction changed. Trajectory classifications were largely unchanged for absolute $\log_2FC > 0.2$: 1,583 of 1,584 originally classified gene–genotype–treatment trajectories retained their class. At absolute $\log_2FC > 0.5$, 1,151 retained their class, and 433 became unclassified (Supplementary File S28).

Fading trajectories were prominent in WT drought, heat, and combination lineages, consistent with many earlier expression differences no longer being detected after stress withdrawal. WT $CO_2$ lineages showed a more pronounced emergent component in G5. In *gsnor-ko*, persistent and switching trajectories were more prominent under $O_3$, heat, and combination conditions, whereas drought was dominated by fading trajectories (Supplementary Fig. S18). Heatmaps of individual



ACCEPTED MANUSCRIPT

Downloaded from academic.oup.com/jxb/advance-article/doi/10.1093/jxb/erag557/9016158 by guest on 12 November 2026

genes supported these scenario-dependent patterns (Supplementary Fig. S19–S22). Thus, altered NO homeostasis was associated with distinct trajectories of transcriptional responses rather than with a uniform increase in recurrence across sampled generations and treatments.

## 4.2 Recurrently responsive transcription factors identify candidate regulatory nodes

To identify responses recurrently detected at G1, G3, and G5, we extracted transcription factors (TFs) that were differentially expressed across all three analysed generations within each treatment and visualised their expression patterns across genotypes and environments (Supplementary Fig. S23). This analysis showed that persistent responses were not limited to downstream functional genes but also involved multiple TF families, suggesting that part of the similar differential expression states were detected at multiple sampling points at the regulatory level.

Across treatments, recurrently responsive TFs belonged to several well-established stress-associated families, including basic helix-loop-helix (bHLH), basic leucine zipper (bZIP), ERF, MYB, WRKY, homeodomain-leucine zipper (HD-ZIP), GAI-RGA-SCR (GRAS), nuclear factor Y (NF-Y), and CONSTANS-like (CO-like) groups. Representative candidates included BRI1-EMS-SUPPRESSOR 1 (BES1), bHLH and ERF family members, MYB-related genes, WRKY transcription factors, NF-YB subunits, and TEOSINTE BRANCHED1/CYCLOIDEA/PROLIFERATING CELL FACTOR (TCP) factors, highlighting regulatory programs potentially associated with stable stress adaptation across generations (references/PubMed IDs in Supplementary File S20). These signatures were most prominent under heat and combination conditions in WT and under $O_3$, heat, and combination conditions in *gsnor-ko*. The candidate genes indicate that recurrent expression responses include potential regulators, although their causal roles remain to be tested.

## 4.3 Candidate epigenetic regulators occur in recurrent and switching expression patterns

The enrichment of chromatin- and RNA-associated functions prompted us to examine stress-responsive genes with reported roles in these processes. Based on published gene functions, we organised the candidates into five, potentially overlapping regulatory models: DNA methylation and heterochromatin regulation (Model 1), Polycomb-associated repression (Model 2), H2B ubiquitination and chromatin regulation (Model 3), $m^6A$ RNA methylation (Model 4), and one-

ACCEPTED MANUSCRIPT

Downloaded from academic.oup.com/jxb/advance-article/doi/10.1093/jxb/erag557/9016158 by guest on 12 November 2026

carbon metabolism (Model 5). We then visualised each gene's expression pattern across treatments, generations, and genotypes (Figs 5–6). These models are literature-informed functional groupings; membership does not require a persistent or switching trajectory. Gene-specific patterns and supporting references are provided in Supplementary File S21.

The first group comprised genes associated with the establishment and reinforcement of DNA methylation, as well as heterochromatin compaction (Model 1). This group included RNA-DEPENDENT RNA POLYMERASE 2 (RDR2), ARGONAUTE 6 (AGO6), DEFECTIVE IN MERISTEM SILENCING 3 (DMS3), CHROMOMETHYLASE 3 (CMT3), MICRORCHIDIA 3/6 (MORC3/6), AGENET DOMAIN CONTAINING PROTEIN 1 (ADCP1), DECREASE IN DNA METHYLATION 1 (DDM1), H2A.W histone variants, DOMAINS REARRANGED METHYLTRANSFERASE 2 (DRM2), and RNA-DIRECTED DNA METHYLATION 1 (RDM1) (Fig. 5A and 6A). These candidates were differentially expressed across multiple stress trajectories, with particularly prominent changes under heat and combination in WT, and under elevated $O_3$, heat, and combination in *gsnor-ko*. The occurrence of both positive and negative changes within this group suggests dynamic remodelling rather than a uniform directional response.

Genes associated with Polycomb-mediated repression and H3K27me3-linked regulation (Model 2), including BASIC PENTACYSTEINE 1/2/3 (BPC1/2/3), CURLY LEAF (CLF), FERTILIZATION-INDEPENDENT ENDOSPERM (FIE), and MULTICOPY SUPPRESSOR OF IRA 1 (MSI1), showed a more selective and generally weaker transcriptional response (Fig. 5B and 6B). Nevertheless, recurrent changes in this group, particularly under the combination scenario in WT and under $O_3$, heat, and combination in *gsnor-ko*, indicate that Polycomb-related pathways may also contribute to stable or reconfigured transcriptional states across generations.

A third group comprised genes involved in H2B ubiquitination and chromatin resetting (Model 3), including UBIQUITIN-SPECIFIC PROTEASE 22 (UBP22), DE-ETIOLATED 1 (DET1), HISTONE MONOUBIQUITINATION 1 (HUB1), and HISTONE MONOUBIQUITINATION 2 (HUB2), together with several HISTONE H2B genes (Fig. 5C and 6C). These genes again showed broader perturbation in *gsnor-ko* than in WT, especially under $O_3$, heat, and combination, suggesting an altered chromatin-resetting capacity in the mutant background.

ACCEPTED MANUSCRIPT

Downloaded from academic.oup.com/jxb/advance-article/doi/10.1093/jxb/erag557/9016158 by guest on 12 November 2026

We also identified stress-responsive genes linked to $m^6A$ RNA-methylation-related regulation (Model 4), including ALKB HOMOLOG 10B (ALKBH10B), FKBP12-INTERACTING PROTEIN 37 (FIP37), and mRNA ADENOSINE METHYLASE A (MTA), as well as genes associated with one-carbon metabolism and methyl-donor availability (Model 5), including S-ADENOSYLMETHIONINE SYNTHETASE 4 (SAMS4), S-ADENOSYL-L-HOMOCYSTEINE HYDROLASE 2 (SAHH2), METHYLENETETRAHYDROFOLATE DEHYDROGENASE/METHENYLTETRAHYDROFOLATE CYCLOHYDROLASE 1 (MTHFD1), FOLYLPOLYGLUTAMATE SYNTHETASE 2 (FPGS2), METHYLENETETRAHYDROFOLATE REDUCTASE 2 (MTHFR2), and CYSTATHIONINE GAMMA-SYNTHASE 1 / METHIONINE OVERACCUMULATOR 1 (CGS1/MTO1) (Fig. 5D-E and 6D-E). Although these groups were smaller, they recurred across several stress trajectories, again most clearly under heat and combination in WT and under $O_3$, heat, and combination in *gsnor-ko*.

Overall, these candidate genes were not confined to a single environmental scenario or regulatory class but recurred across multiple trajectories and mechanistic categories. Importantly, the response was broader in *gsnor-ko* than in WT, particularly after a return to control conditions for two generations, consistent with previous findings and indicating reduced transcriptomic resetting in the mutant. However, differential expression alone does not establish epigenetic causality, but the repeated appearance of genes linked to DNA methylation, heterochromatin maintenance, Polycomb repression, histone ubiquitination, RNA methylation, and methyl-donor metabolism supports the idea that chromatin- and RNA-associated regulatory pathways contribute to the maintenance or resetting of environmental responses across generations.

## 4.4 Co-expression network analysis identifies genotype- and generation-associated modules

WGCNA identified modules whose eigengene patterns were primarily associated with genotype or generation, with a clearer treatment-related signal in the ivory module (Supplementary Figs. S24–S29). Functional enrichment linked these modules to development, photosynthesis, respiration, and responses to external stimuli (Supplementary Fig. S26 and S29). Exploratory associations between modules and rosette area or seed weight were heterogeneous and did not reveal robust module–phenotype relationships (Supplementary Fig. S28B–S29A–B).

ACCEPTED MANUSCRIPT

Downloaded from academic.oup.com/jxb/advance-article/doi/10.1093/jxb/erag557/9016158 by guest on 12 November 2026

Because the ivory module included defence-related functions, we also examined pathogen responses (Supplementary Fig. S29–S30). Under control conditions, *gsnor-ko* generally supported greater bacterial growth than WT. In some generations, however, a combination-stress history was associated with reduced bacterial growth in *gsnor-ko* relative to its corresponding control history (Supplementary Fig. S30A–B; Supplementary File S22). These exploratory leaf-level observations varied with generation and genotype; plant-level inference is limited because leaves could not be linked to individual plants.

# Discussion

*Arabidopsis thaliana* was repeatedly exposed to future climate conditions for 3 generations, followed by 2 generations grown under control conditions, and phenotypic, transcriptomic, and network-level analyses were performed. A central outcome of this study is that both genotype background and stress context shaped the extent of recovery after repeated perturbations. In WT, many responses returned to a control-like state after stress withdrawal, whereas *gsnor-ko* more often retained reduced growth, low seed production, and altered transcriptional states. These observations are consistent with a contribution of GSNOR-dependent NO/redox homeostasis to transcriptional recovery.

## 1. GSNOR deficiency is associated with altered recovery after repeated climate stress

Across the phenotypic datasets, repeated climate stress revealed a clear genotype-dependent difference in recovery across generations rather than a single uniform stress effect. Because *gsnor-ko* was smaller than WT even under control conditions, we interpreted treatment-related rosette recovery using responses normalised to the corresponding control within each genotype and generation (Supplementary Fig. S8). Absolute differences between WT and *gsnor-ko* were considered alongside these responses because they also reflect the mutant's baseline growth phenotype. This is consistent with earlier work showing that GSNOR is required for normal growth/development and thermotolerance, and with later evidence linking NO/GSNOR signalling to chromatin-associated regulation of stress responses (Ageeva-Kieferle *et al.*, 2021; Rudolf *et al.*, 2021; Lee *et al.*, 2008).

ACCEPTED MANUSCRIPT

Downloaded from academic.oup.com/jxb/advance-article/doi/10.1093/jxb/erag557/9016158 by guest on 12 November 2026

The measured traits differed in their degree of plasticity. Rosette area showed the clearest genotype-, generation-, and treatment-dependent patterns, whereas QYmax remained comparatively stable, and NPQ_Lss captured changes in energy dissipation. Seed production further distinguished the genotypes: WT often showed higher yield after stress withdrawal, whereas *gsnor-ko* remained low across treatments and generations. Similar phenotypic responses for *gsnor-ko* have been reported before in response to biotic stress (Holzmeister *et al.*, 2011).

A limitation of the design is that environmental treatments were assigned to fixed subchambers and were not replicated across independent environmental units within a generation. Treatment differences, particularly comparisons between the ambient and heat chambers, may therefore include chamber or subchamber effects. Our treatment-level findings should be interpreted as responses under the implemented climate scenarios rather than estimates from independently replicated chamber treatments. Genotype comparisons within a scenario are less directly affected because WT and *gsnor-ko* were co-grown in the same subchamber, although the generality of those comparisons across independent chamber environments remains untested.

Because generations were grown sequentially, the generation and experimental date cannot be separated completely. The reduction in the control rosette area in G3 suggests that a generation-wide factor may have contributed to the differences in growth. The available data do not establish whether this reflected seasonal influences or another change between experimental runs.

Among the tested scenarios, $O_3$, heat, and the combination treatment were especially informative because they are closely linked to redox and nitrosative signalling. $O_3$ activates ROS-, NO-, salicylic acid-, and ethylene-linked pathways in Arabidopsis (Ahlfors *et al.*, 2009), while heat is the context in which GSNOR function has been most clearly linked to stress tolerance and thermomemory-related processes (Lee *et al.*, 2008; Naaz *et al.*, 2025). The strong genotype dependence of these scenarios therefore fits a model in which GSNO homeostasis contributes not only to immediate stress responses, but also to the maintenance or clearance of their downstream consequences.

The multigenerational design also introduces dependence among descendants of the same progenitor. Although sampling across the recorded pedigrees was generally balanced (Supplementary File S24), pedigree and immediate-parent identity were not included in the

ACCEPTED MANUSCRIPT

Downloaded from academic.oup.com/jxb/advance-article/doi/10.1093/jxb/erag557/9016158 by guest on 12 November 2026

original phenotypic or RNA-seq models. Consequently, the reported statistical tests may overstate the precision of comparisons involving multiple plants from the same lineage. We interpret the patterns across generations with this limitation in mind; their robustness to pedigree-level analysis remains to be tested.

2. Multi-generational transcriptome responses distinguish resetting from persistence

The RNA-seq data showed high mapping quality and reproducible multivariate structure, supporting the interpretation that the observed transcriptional patterns are biological rather than technical. More importantly, DAPC and PCA indicated that genotype background and generation contributed more strongly to global transcriptome organisation than any single treatment snapshot. This suggests that a history of repeated stress becomes embedded in the transcriptome as a state variable, rather than appearing only as a transient response in individual contrasts. This systems-level structure is compatible with the broader molecular-memory literature, such as work in poplar under future-climate-relevant drought and heat scenarios, which showed that transcriptomes can differ most strongly during recovery rather than during the stress exposure itself, highlighting post-stress state transitions as a major component of climate resilience (Georgii *et al.*, 2019).

RNA-seq was performed in G1, G3, and G5, but not in G2 or G4. Thus, detection of the same differential-expression state at all three sampled points demonstrates recurrence at those points, not uninterrupted maintenance across the intervening generations. Similarly, a G5 response after two control-grown generations does not reveal whether that response persisted through G4 or re-emerged by G5. The absence of a significant difference at G5 indicates that an earlier response was no longer detected, rather than establishing when or how resetting occurred. For example, in WT, drought, heat, and the combination treatment generally showed declining DEG numbers across generations, and the gene-state analysis indicated fading as a dominant trajectory in several of these conditions. Together, these patterns are consistent with fewer detectable stress-associated differences in expression at the G5 sampling point. By contrast, *gsnor-ko* showed altered DEG magnitude, altered temporal profiles, and broader persistent or switcher behaviour, particularly under $O_3$, heat, and combination scenarios, consistent with the view that NO is a central node in plant responses to both elevated greenhouse-gas-related environments and ozone-linked oxidative signalling (Kabange *et al.*, 2022). Thus, the mutant differed from WT not only in response strength but also in the expression states detected at G1, G3 and G5.

ACCEPTED MANUSCRIPT

Downloaded from academic.oup.com/jxb/advance-article/doi/10.1093/jxb/erag557/9016158 by guest on 12 November 2026

Importantly, the combined treatment should not be viewed simply as a stronger version of the single stresses. In Arabidopsis, combined stresses frequently generate transcriptomic and metabolic responses that are not predictable from single-stress experiments alone (Rasmussen *et al.*, 2013; Zinta *et al.*, 2018). In our dataset, the single treatments helped resolve pathway-specific behaviour—for example, drought- and $CO_2$-related shifts versus the more strongly redox-linked $O_3$ and heat responses—whereas the combination treatment provided a test of how plants integrate overlapping stress cues and how effectively they reset once stress is removed. The fact that *gsnor-ko* remained more altered than WT under the combination regime, therefore, supports the idea that NO-mediated signalling is particularly important when multiple stress signals converge.

These findings align with current views of stress memory, in which recovery is an active process and persistent molecular responses do not, by themselves, establish stable meiotic inheritance (Crisp et al., 2016; Harris et al., 2023; Hemenway and Gehring, 2023; Oberkofler et al., 2021). Studies of heat-stress memory likewise highlight chromatin-associated resetting as a determinant of whether stress-responsive states persist or are cleared (Iwasaki and Paszkowski, 2014; Pratx et al., 2024; Staacke et al., 2025).

### 3. Chromatin-, RNA-, and methylation-linked signatures nominate candidate mechanisms

The enrichment analyses nominate regulatory pathways that may contribute to the observed transcriptional responses. Both genotypes shared a core set of responses involving photosynthesis, glutaredoxin, S-glutathionylation, nutrient uptake, SnRK1-linked regulation, and stress-associated transcription factors, indicating that repeated climate stress engages overlapping energetic, redox, and regulatory programs. However, the more informative result is that *gsnor-ko* showed broader or stronger recurrence of terms associated with DNA methylation, heterochromatin maintenance, RdDM-linked regulation, histone organisation, ubiquitin-mediated chromatin control, RNA modification, and methyl-donor metabolism.

Although the enrichments analysis does not demonstrate that a specific chromatin mark or methylation state was inherited across meiosis, it supports the idea that repeated stress engages regulatory layers capable of stabilising or clearing transcriptional states. This interpretation is consistent with work showing that NO can influence chromatin regulation through histone modifications and altered DNA accessibility, and that GSNOR contributes to demethylation-associated regulation of transposable elements and stress-responsive genes (Ageeva-Kieferle *et*

ACCEPTED MANUSCRIPT

Downloaded from academic.oup.com/jxb/advance-article/doi/10.1093/jxb/erag557/9016158 by guest on 12 November 2026

*al.*, 2021; Rudolf *et al.*, 2021). It is also compatible with current models of abiotic-stress memory in which DNA methylation, histone dynamics, non-coding RNAs, RNA turnover, and RNA-directed silencing act together to shape the intensity and duration of memory (Crisp *et al.*, 2016; Cao and Chen, 2024; Xu *et al.*, 2024; Kaya and Adamakis, 2025).

In this context, the candidate regulators identified in our dataset, including factors linked to RdDM and heterochromatin reinforcement, histone ubiquitination, Polycomb-related repression, RNA methylation, and one-carbon metabolism, provide a plausible mechanistic bridge between altered redox signalling and reduced transcriptomic resetting in *gsnor-ko*.

## 4. Conclusions and Outlook

Taken together, the phenotypic and transcriptomic differences are consistent with a model in which GSNOR activity contributes to recovery after repeated climate stress. The treatment-associated expression states detected in WT and *gsnor-ko* differed according to stress scenario and sampled generation. However, this study examined a single *gsnor1-3* allele without an independent allele or genetic complementation. The mutant also differed markedly from WT in growth and reproductive output under control conditions. Consequently, we cannot distinguish a direct effect of GSNOR-dependent signalling on transcriptomic recovery from effects mediated by the mutant's constitutive developmental or physiological state. Testing independent alleles or complemented lines would help resolve this distinction.

This model is relevant in the context of future climate change, where recurrent and overlapping stresses are expected to become more common, and resilience will depend not only on acute tolerance but also on how efficiently plants recover between stress episodes. In that sense, our study complements work on future-climate molecular memory by identifying NO homeostasis as a candidate contributor to variation in post-stress recovery (Fejes *et al.*, 2025; Georgii *et al.*, 2019; Peer, 2026).

Direct testing of this model will require profiling DNA methylation, chromatin accessibility, histone modifications, and small RNAs within the same multigenerational framework. Functional tests of the candidate regulators identified here could then establish whether chromatin-, RNA-, and methyl-donor-related pathways contribute causally to GSNOR-dependent recovery. Until such evidence is available, our results support multigenerational differences in transcriptional

ACCEPTED MANUSCRIPT

Downloaded from academic.oup.com/jxb/advance-article/doi/10.1093/jxb/erag557/9016158 by guest on 12 November 2026

persistence and resetting, rather than proof of transgenerational epigenetic inheritance (Supplementary Fig. S31).

# Acknowledgements

This work (for RB and CL) was supported by the Initiative and Networking Fund of the Helmholtz Association under the call HIRS, the EpiCrossBorders: International Helmholtz-Edinburgh Research School for Epigenetics, Biotechnology and UK Research and Innovation (UKRI) Biological Sciences Research Council (BBSRC) grant BB/S010262/1 (to LF) and by the European Research Council (ERC) under the European Union's Horizon 2020 research and innovation program, grant agreement no. 101001137 (to SHS.).

We thank Peiyuan Zhu, Moritz Popp, Ina Zimmer, Petra Seibel, Franz Buegger, Mustafa Oezden, Alexandros Sigalas, Georg Gerl, Ulrich Junghans, Baris Weber, and Armin Richter for their technical support during experimental work, and Tetyana Nosenko for helping with RNA-seq data pre-processing. We thank Dr. Sophie Haupt and her team at the Plant Growth Facilities of the School of Biological Sciences, University of Edinburgh. We would also like to thank Prof. Dr. Aloys Schepers for his fruitful input during thesis meetings.

During the preparation of this work, the author(s) used AI tools (such as ChatGPT 5.4 and Grammarly 1.162.2.0) in order to polish the writing framework and search relevant research articles (literature overview). After using this tool/service, the author(s) reviewed and edited the content as needed and take(s) full responsibility for the content of the published article.

# Author contributions

Experiments were designed by CL & FJ; experimental work was conducted by RB, AG, JBW, EM, LG, AA, CL & JPS. Analysis was performed by RB; statistical analysis and RNA-seq analysis support were provided by SJ, KFXM, and JPS; disease assays and analysis were performed by LF, SHS & RB; seed phenotyping and analysis were performed by AF, GH & RK; data interpretation was performed by RB, LF & JPS; and the paper was written by RB with input from JPS, AG, BJW, CL, LF, FJ & KFXM. The written paper was reviewed by all the co-authors.

ACCEPTED MANUSCRIPT

Downloaded from academic.oup.com/jxb/advance-article/doi/10.1093/jxb/erag557/9016158 by guest on 12 November 2026

# Conflict of interest

Not declared

# Data availability

The raw RNA-seq sequencing data supporting this study have been deposited in ArrayExpress under accession **E-MTAB-17127**. Processed data and associated supporting materials, including phenotypic data, the RNA-seq count matrix, supplementary files, R scripts and FastQC quality-control reports, have been deposited in Zenodo: https://doi.org/10.5281/zenodo.22960793.

# References


**Ageeva-Kieferle A, Georgii E, Winkler B, Ghirardo A, Albert A, Hüther P, Mengel A, Becker C, Schnitzler JP, Durner J, Lindermayr C**. 2021. Nitric oxide coordinates growth, development, and stress response via histone modification and gene expression. Plant Physiol **187**, 336-360.

**Ahlfors R, Brosché M, Kollist H, Kangasjärvi J**. 2009. Nitric oxide modulates ozone-induced cell death, hormone biosynthesis and gene expression in Arabidopsis thaliana. Plant J **58**, 1-12.

**Baker NR**. 2008. Chlorophyll fluorescence: a probe of photosynthesis in vivo. Annu Rev Plant Biol **59**, 89-113.

**Bayerisches Staatsministerium für Umwelt und Verbraucherschutz**. 2021. Klima-Report Bayern 2021: Klimawandel, Auswirkungen, Anpassungs- und Forschungsaktivitäten. München: Bayerisches Staatsministerium für Umwelt und Verbraucherschutz.

**Behl R, Gallo-Franco JJ, Hazarika RR, Zhang Z, Wilming F, Schnitzler JP, Lindermayr C, Johannes F**. 2026. DNA methylome responses to biotic and abiotic stress in Arabidopsis thaliana: A multi-study analysis. Plant Biol (Stuttg).

**Boyko A, Blevins T, Yao Y, Golubov A, Bilichak A, Ilnytskyy Y, Hollunder J, Meins F, Jr., Kovalchuk I**. 2010. Transgenerational adaptation of Arabidopsis to stress requires DNA methylation and the function of Dicer-like proteins. PLoS One **5**, e9514.

**Brzezinka K, Altmann S, Czesnick H, Nicolas P, Gorka M, Benke E, Kabelitz T, Jähne F, Graf A, Kappel C, Bäurle I**. 2016. Arabidopsis FORGETTER1 mediates stress-induced chromatin memory through nucleosome remodeling. Elife **5**.


ACCEPTED MANUSCRIPT

Downloaded from academic.oup.com/jxb/advance-article/doi/10.1093/jxb/erag557/9016158 by guest on 12 November 2026

**Cao S, Chen ZJ**. 2024. Transgenerational epigenetic inheritance during plant evolution and breeding. Trends Plant Sci **29**, 1203-1223.

**Chen R, Sun S, Wang C, Li Y, Liang Y, An F, Li C, Dong H, Yang X, Zhang J, Zuo J**. 2009. The Arabidopsis PARAQUAT RESISTANT2 gene encodes an S-nitrosoglutathione reductase that is a key regulator of cell death. Cell Res **19**, 1377-1387.

**Chomczynski P, Sacchi N**. 1987. Single-step method of RNA isolation by acid guanidinium thiocyanate-phenol-chloroform extraction. Anal Biochem **162**, 156-159.

**Crisp PA, Ganguly D, Eichten SR, Borevitz JO, Pogson BJ**. 2016. Reconsidering plant memory: Intersections between stress recovery, RNA turnover, and epigenetics. Sci Adv **2**, e1501340.

**De Kauwe MG, Medlyn BE, Tissue DT**. 2021. To what extent can rising [CO(2) ] ameliorate plant drought stress? New Phytol **231**, 2118-2124.

**Delledonne M, Xia Y, Dixon RA, Lamb C**. 1998. Nitric oxide functions as a signal in plant disease resistance. Nature **394**, 585-588.

**Deutscher Wetterdienst**. 2026. München (Flugh.) climate table and station metadata [WWW document]. Offenbach, Germany: Deutscher Wetterdienst.

**Durner J, Wendehenne D, Klessig DF**. 1998. Defense gene induction in tobacco by nitric oxide, cyclic GMP, and cyclic ADP-ribose. Proc Natl Acad Sci U S A **95**, 10328-10333.

**Erdmann RM, Picard CL**. 2020. RNA-directed DNA Methylation. PLoS Genet **16**, e1009034.

**Feechan A, Kwon E, Yun BW, Wang Y, Pallas JA, Loake GJ**. 2005. A central role for S-nitrosothiols in plant disease resistance. Proc Natl Acad Sci U S A **102**, 8054-8059.

**Fejes G, Bodor T, Szőllősi R, Kondak S, Kutasi K, Fotopoulos V, Kolbert Z**. 2025. Nitric oxide as an integral element in priming-induced tolerance and plant stress memory. J Exp Bot **76**, 3669-3685.

**Fitzky AC, Sandén H, Karl T, Fares S, Calfapietra C, Grote R, Saunier A, Rewald B**. 2019. The Interplay Between Ozone and Urban Vegetation—BVOC Emissions, Ozone Deposition, and Tree Ecophysiology. Frontiers in Forests and Global Change **Volume 2 - 2019**.

**Friedrich T, Oberkofler V, Trindade I, Altmann S, Brzezinka K, Lämke J, Gorka M, Kappel C, Sokolowska E, Skirycz A, Graf A, Bäurle I**. 2021. Heteromeric HSFA2/HSFA3 complexes drive transcriptional memory after heat stress in Arabidopsis. Nat Commun **12**, 3426.

ACCEPTED MANUSCRIPT

Downloaded from academic.oup.com/jxb/advance-article/doi/10.1093/jxb/erag557/9016158 by guest on 12 November 2026

**Frungillo L, Oka N, Lee S-U, Nomoto M, Yun B-W, Tada Y, Spoel SH**. 2023. The pathogenic coronatine toxin hijacks host redox signalling to suppress plant immunity. bioRxiv, 2023.2012.2001.569535.

**Ganguly DR, Crisp PA, Eichten SR, Pogson BJ**. 2017. The Arabidopsis DNA Methylome Is Stable under Transgenerational Drought Stress. Plant Physiol **175**, 1893-1912.

**Georgii E, Kugler K, Pfeifer M, Vanzo E, Block K, Domagalska MA, Jud W, AbdElgawad H, Asard H, Reinhardt R, Hansel A, Spannagl M, Schäffner AR, Palme K, Mayer KFX, Schnitzler JP**. 2019. The Systems Architecture of Molecular Memory in Poplar after Abiotic Stress. Plant Cell **31**, 346-367.

**Ghirardo A, Lindstein F, Koch K, Buegger F, Schloter M, Albert A, Michelsen A, Winkler JB, Schnitzler JP, Rinnan R**. 2020. Origin of volatile organic compound emissions from subarctic tundra under global warming. Glob Chang Biol **26**, 1908-1925.

**Harris CJ, Amtmann A, Ton J**. 2023. Epigenetic processes in plant stress priming: Open questions and new approaches. Curr Opin Plant Biol **75**, 102432.

**Hemenway EA, Gehring M**. 2023. Epigenetic Regulation During Plant Development and the Capacity for Epigenetic Memory. Annu Rev Plant Biol **74**, 87-109.

**Holzmeister C, Fröhlich A, Sarioglu H, Bauer N, Durner J, Lindermayr C**. 2011. Proteomic analysis of defense response of wildtype Arabidopsis thaliana and plants with impaired NO-homeostasis. Proteomics **11**, 1664-1683.

**Im U, Incecik S, Guler M, Tek A, Topcu S, Unal YS, Yenigun O, Kindap T, Odman MT, Tayanc M**. 2013. Analysis of surface ozone and nitrogen oxides at urban, semi-rural and rural sites in Istanbul, Turkey. Sci Total Environ **443**, 920-931.

**IPCC**. 2023a. Weather and Climate Extreme Events in a Changing Climate. In: Intergovernmental Panel on Climate C, ed. *Climate Change 2021 – The Physical Science Basis: Working Group I Contribution to the Sixth Assessment Report of the Intergovernmental Panel on Climate Change*. Cambridge: Cambridge University Press, 1513-1766.

**IPCC**. 2023b. Climate Change Information for Regional Impact and for Risk Assessment. In: Intergovernmental Panel on Climate C, ed. *Climate Change 2021 – The Physical Science Basis: Working Group I Contribution to the Sixth Assessment Report of the Intergovernmental Panel on Climate Change*. Cambridge: Cambridge University Press, 1767-1926.

ACCEPTED MANUSCRIPT

Downloaded from academic.oup.com/jxb/advance-article/doi/10.1093/jxb/erag557/9016158 by guest on 12 November 2026

**Iwasaki M, Paszkowski J**. 2014. Identification of genes preventing transgenerational transmission of stress-induced epigenetic states. Proc Natl Acad Sci U S A **111**, 8547-8552.

**Jahnke S, Roussel J, Hombach T, Kochs J, Fischbach A, Huber G, Scharr H**. 2016. phenoSeeder - A Robot System for Automated Handling and Phenotyping of Individual Seeds. Plant Physiol **172**, 1358-1370.

**Jensen DE, Belka GK, Du Bois GC**. 1998. S-Nitrosoglutathione is a substrate for rat alcohol dehydrogenase class III isoenzyme. Biochem J **331 ( Pt 2)**, 659-668.

**Kabange NR, Mun BG, Lee SM, Kwon Y, Lee D, Lee GM, Yun BW, Lee JH**. 2022. Nitric oxide: A core signaling molecule under elevated GHGs (CO(2), CH(4), N(2)O, O(3))-mediated abiotic stress in plants. Front Plant Sci **13**, 994149.

**Kaya C, Adamakis IS**. 2025. Redox-Epigenetic Crosstalk in Plant Stress Responses: The Roles of Reactive Oxygen and Nitrogen Species in Modulating Chromatin Dynamics. Int J Mol Sci **26**, 7167.

**Klasen D, Fischbach A, Sydoruk V, Kochs J, Bühler J, Koller R, Huber G**. 2025. Seed-to-plant-tracking: automated phenotyping of seeds and corresponding plants of Arabidopsis. Front Plant Sci **16**, 1539424.

**Korotko U, Chwiałkowska K, Sańko-Sawczenko I, Kwasniewski M**. 2021. DNA Demethylation in Response to Heat Stress in Arabidopsis thaliana. Int J Mol Sci **22**.

**Langfelder P, Zhang B, Horvath S**. 2008. Defining clusters from a hierarchical cluster tree: the Dynamic Tree Cut package for R. Bioinformatics **24**, 719-720.

**Langfelder P, Horvath S**. 2008. WGCNA: an R package for weighted correlation network analysis. BMC Bioinformatics **9**, 559.

**Lee U, Wie C, Fernandez BO, Feelisch M, Vierling E**. 2008. Modulation of nitrosative stress by S-nitrosoglutathione reductase is critical for thermotolerance and plant growth in Arabidopsis. Plant Cell **20**, 786-802.

**Liao Y, Smyth GK, Shi W**. 2013. featureCounts: an efficient general purpose program for assigning sequence reads to genomic features. Bioinformatics **30**, 923-930.

**Lindermayr C, Rudolf EE, Durner J, Groth M**. 2020. Interactions between metabolism and chromatin in plant models. Mol Metab **38**, 100951.

**Lindermayr C, Sell S, Müller B, Leister D, Durner J**. 2010. Redox Regulation of the NPR1-TGA1 System of Arabidopsis thaliana by Nitric Oxide The Plant Cell **22**, 2894-2907.

ACCEPTED MANUSCRIPT

Downloaded from academic.oup.com/jxb/advance-article/doi/10.1093/jxb/erag557/9016158 by guest on 12 November 2026

**Liu L, Hausladen A, Zeng M, Que L, Heitman J, Stamler JS**. 2001. A metabolic enzyme for S-nitrosothiol conserved from bacteria to humans. Nature **410**, 490-494.

**Liu HC, Lämke J, Lin SY, Hung MJ, Liu KM, Charng YY, Bäurle I**. 2018. Distinct heat shock factors and chromatin modifications mediate the organ-autonomous transcriptional memory of heat stress. Plant J **95**, 401-413.

**Liu R, Lang Z**. 2020. The mechanism and function of active DNA demethylation in plants. J Integr Plant Biol **62**, 148-159.

**Meinshausen M, Nicholls ZRJ, Lewis J, Gidden MJ, Vogel E, Freund M, Beyerle U, Gessner C, Nauels A, Bauer N, Canadell JG, Daniel JS, John A, Krummel PB, Luderer G, Meinshausen N, Montzka SA, Rayner PJ, Reimann S, Smith SJ, van den Berg M, Velders GJM, Vollmer MK, Wang RHJ**. 2020. The shared socio-economic pathway (SSP) greenhouse gas concentrations and their extensions to 2500. Geosci. Model Dev. **13**, 3571-3605.

**Miller G, Schlauch K, Tam R, Cortes D, Torres MA, Shulaev V, Dangl JL, Mittler R**. 2009. The plant NADPH oxidase RBOHD mediates rapid systemic signaling in response to diverse stimuli. Sci Signal **2**, ra45.

**Molinier J, Ries G, Zipfel C, Hohn B**. 2006. Transgeneration memory of stress in plants. Nature **442**, 1046-1049.

**Montes CM, Demler HJ, Li S, Martin DG, Ainsworth EA**. 2022. Approaches to investigate crop responses to ozone pollution: from O(3) -FACE to satellite-enabled modeling. Plant J **109**, 432-446.

**Murchie EH, Lawson T**. 2013. Chlorophyll fluorescence analysis: a guide to good practice and understanding some new applications. J Exp Bot **64**, 3983-3998.

**Naaz S, Pande A, Laxmi A**. 2025. Nitric oxide-mediated thermomemory: a new perspective on plant heat stress resilience. Front Plant Sci **16**, 1525336.

**Nishio H, Kawakatsu T, Yamaguchi N**. 2024. Beyond heat waves: Unlocking epigenetic heat stress memory in Arabidopsis. Plant Physiol **194**, 1934-1951.

**Nunez-Vazquez R, Desvoyes B, Gutierrez C**. 2022. Histone variants and modifications during abiotic stress response. Front Plant Sci **13**, 984702.

**Oberkofler V, Pratx L, Bäurle I**. 2021. Epigenetic regulation of abiotic stress memory: maintaining the good things while they last. Curr Opin Plant Biol **61**, 102007.

ACCEPTED MANUSCRIPT

Downloaded from academic.oup.com/jxb/advance-article/doi/10.1093/jxb/erag557/9016158 by guest on 12 November 2026

**Pardal AJ, Piquerez SJM, Dominguez-Ferreras A, Frungillo L, Mastorakis E, Reilly E, Latrasse D, Concia L, Gimenez-Ibanez S, Spoel SH, Benhamed M, Ntoukakis V**. 2021. Immunity onset alters plant chromatin and utilizes EDA16 to regulate oxidative homeostasis. PLoS Pathog **17**, e1009572.

**Pascual LS, Segarra-Medina C, Gómez-Cadenas A, López-Climent MF, Vives-Peris V, Zandalinas SI**. 2022. Climate change-associated multifactorial stress combination: A present challenge for our ecosystems. J Plant Physiol **276**, 153764.

**Peer LA**. 2026. The epigenetic set-point: metabolic and redox gating of developmental transitions in plants. New Phytol.

**Pratx L, Wendering P, Kappel C, Nikoloski Z, Bäurle I**. 2023. Histone retention preserves epigenetic marks during heat stress-induced transcriptional memory in plants. Embo j **42**, e113595.

**Pratx L, Crawford T, Bäurle I**. 2024. Mechanisms of heat stress-induced transcriptional memory. Curr Opin Plant Biol **81**, 102590.

**Rao X, Yang S, Lü S, Yang P**. 2024. DNA Methylation Dynamics in Response to Drought Stress in Crops. Plants (Basel) **13**.

**Rasmussen S, Barah P, Suarez-Rodriguez MC, Bressendorff S, Friis P, Costantino P, Bones AM, Nielsen HB, Mundy J**. 2013. Transcriptome responses to combinations of stresses in Arabidopsis. Plant Physiol **161**, 1783-1794.

**Reichel M, Köster T, Staiger D**. 2019. Marking RNA: m6A writers, readers, and functions in Arabidopsis. J Mol Cell Biol **11**, 899-910.

**Roy J, Rineau F, De Boeck HJ, Nijs I, Pütz T, Abiven S, Arnone JA, 3rd, Barton CVM, Beenaerts N, Brüggemann N, Dainese M, Domisch T, Eisenhauer N, Garré S, Gebler A, Ghirardo A, Jasoni RL, Kowalchuk G, Landais D, Larsen SH, Leemans V, Le Galliard JF, Longdoz B, Massol F, Mikkelsen TN, Niedrist G, Piel C, Ravel O, Sauze J, Schmidt A, Schnitzler JP, Teixeira LH, Tjoelker MG, Weisser WW, Winkler B, Milcu A**. 2021. Ecotrons: Powerful and versatile ecosystem analysers for ecology, agronomy and environmental science. Glob Chang Biol **27**, 1387-1407.

**Rudolf EE, Hüther P, Forné I, Georgii E, Han Y, Hell R, Wirtz M, Imhof A, Becker C, Durner J, Lindermayr C**. 2021. GSNOR Contributes to Demethylation and Expression of Transposable Elements and Stress-Responsive Genes. Antioxidants (Basel) **10**.

ACCEPTED MANUSCRIPT

Downloaded from academic.oup.com/jxb/advance-article/doi/10.1093/jxb/erag557/9016158 by guest on 12 November 2026

**Skelly MJ, Frungillo L, Spoel SH**. 2016. Transcriptional regulation by complex interplay between post-translational modifications. Curr Opin Plant Biol **33**, 126-132.

**Staacke T, Mueller-Roeber B, Balazadeh S**. 2025. Stress resilience in plants: the complex interplay between heat stress memory and resetting. New Phytol **245**, 2402-2421.

**Tada Y, Spoel SH, Pajerowska-Mukhtar K, Mou Z, Song J, Wang C, Zuo J, Dong X**. 2008. Plant immunity requires conformational changes [corrected] of NPR1 via S-nitrosylation and thioredoxins. Science **321**, 952-956.

**Thiel S, Döhring T, Köfferlein M, Kosak A, Martin P, Seidlitz HK**. 1996. A Phytotron for Plant Stress Research: How Far Can Artificial Lighting Compare to Natural Sunlight? Journal of Plant Physiology **148**, 456-463.

**Ueda M, Seki M**. 2020. Histone Modifications Form Epigenetic Regulatory Networks to Regulate Abiotic Stress Response. Plant Physiol **182**, 15-26.

**Vanzo E, Jud W, Li Z, Albert A, Domagalska MA, Ghirardo A, Niederbacher B, Frenzel J, Beemster GT, Asard H, Rennenberg H, Sharkey TD, Hansel A, Schnitzler JP**. 2015. Facing the Future: Effects of Short-Term Climate Extremes on Isoprene-Emitting and Nonemitting Poplar. Plant Physiol **169**, 560-575.

**Xu WB, Cao F, Liu P, Yan K, Guo QH**. 2024. The multifaceted role of RNA-based regulation in plant stress memory. Front Plant Sci **15**, 1387575.

**Yip AM, Horvath S**. 2007. Gene network interconnectedness and the generalized topological overlap measure. BMC Bioinformatics **8**, 22.

**Zheng S, Zhao W, Liu Z, Geng Z, Li Q, Liu B, Li B, Bai J**. 2024. Establishment and Maintenance of Heat-Stress Memory in Plants. Int J Mol Sci **25**.

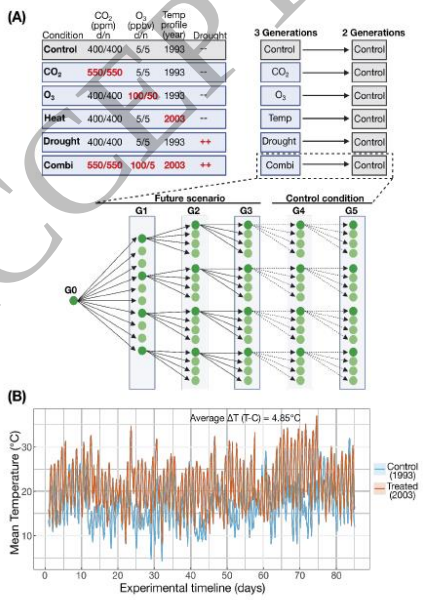
**Zinta G, AbdElgawad H, Peshev D, Weedon JT, Van den Ende W, Nijs I, Janssens IA, Beemster GTS, Asard H**. 2018. Dynamics of metabolic responses to periods of combined heat and drought in Arabidopsis thaliana under ambient and elevated atmospheric CO2. J Exp Bot **69**, 2159-2170.

ACCEPTED MANUSCRIPT

Downloaded from academic.oup.com/jxb/advance-article/doi/10.1093/jxb/erag557/9016158 by guest on 12 November 2026

# Figures

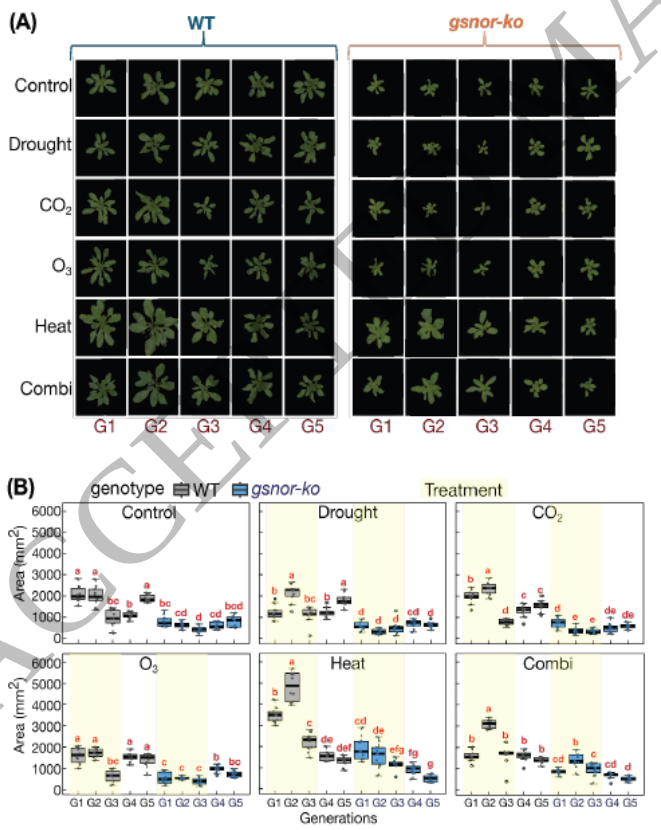
**Fig 1. Experimental design of the multi-generational future-climate study. (A)** Wild type *Arabidopsis thaliana* Col-0 (WT) and the nitric oxide homeostasis mutant *gsnor1-3* (*gsnor-ko*) were propagated across five successive generations (G1-G5) starting from a founder generation (G0). Plants were grown under six climate treatments: control, elevated $CO_2$, elevated $O_3$, heat, drought, and a combined treatment (Combi). Treatments were applied for three consecutive generations (G1-G3), followed by two generations grown under control conditions (G4-G5) to assess the persistence or recovery of stress responses. The environmental regimes for each condition are summarised, including day/night $CO_2$ and $O_3$ concentrations, the annual temperature profile, and drought treatment status. Each environmental treatment occupied one fixed subchamber per generation; treatments were not independently replicated across chambers. WT and *gsnor-ko* were co-grown within each treatment. Phenotyping sampled 10 plants per genotype × treatment × generation. RNA-seq sampled four plants per non-control group in G1, G3 and G5; control groups contained five plants, except WT G1, which contained six. Plants sampled within a subchamber do not constitute independent replicates of the environmental treatment. **(B)** Temperature profiles used for the ExpoSCREEN simulations. Control conditions followed the 1993 temperature profile, whereas the treated warm treatment followed the 2003 profile. The treated profile was, on average, ~5°C warm than the control profile over the experimental timeline. **ALT TEXT:** Diagram of a five-generation Arabidopsis experiment comparing control, drought, elevated carbon dioxide, ozone, heat, and combination treatments followed by two recovery generations.




ACCEPTED MANUSCRIPT

Downloaded from academic.oup.com/jxb/advance-article/doi/10.1093/jxb/erag557/9016158 by guest on 12 November 2026

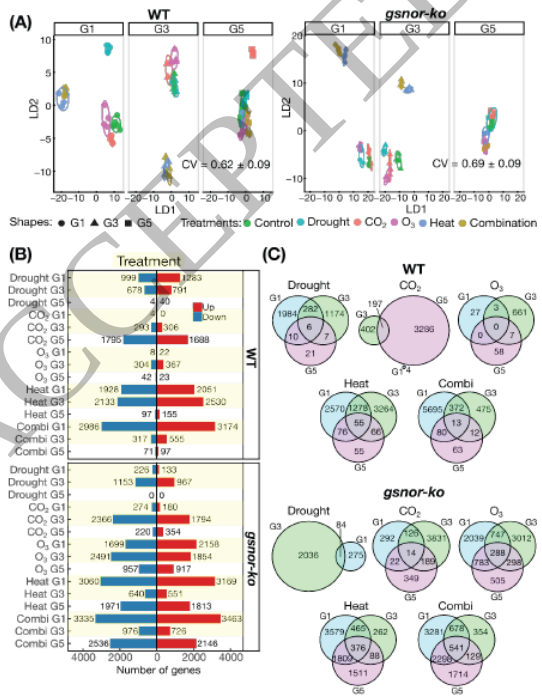
**Fig 2. Multi-generational phenotypic responses of WT and *gsnor-ko* at week 4. (A)** Representative rosette images of WT and *gsnor-ko* plants grown under Control, Drought, elevated $CO_2$, elevated $O_3$, Heat, and Combination treatments across generations G1-G5. **(B)** Rosette area at week 4. Points represent individual plants; 10 plants were sampled per genotype × treatment × generation. Boxes indicate the median and interquartile range. Within each treatment, data were analysed using a Gaussian generalised linear model with genotype, generation and their interaction, followed by Tukey-adjusted pairwise comparisons of estimated marginal means. Groups sharing a letter are not significantly different at adjusted $P < 0.05$. Beige shading identifies G1–G3, when treatment treatments were applied; G4–G5 were grown under control conditions. Each treatment occupied one fixed subchamber per generation, without independent environmental replication. **ALT TEXT:** Rosette images and boxplots show genotype, treatment, and generation dependent growth, with smaller *gsnor* knockout plants and variable recovery after stress withdrawal.




ACCEPTED MANUSCRIPT

Downloaded from academic.oup.com/jxb/advance-article/doi/10.1093/jxb/erag557/9016158 by guest on 12 November 2026

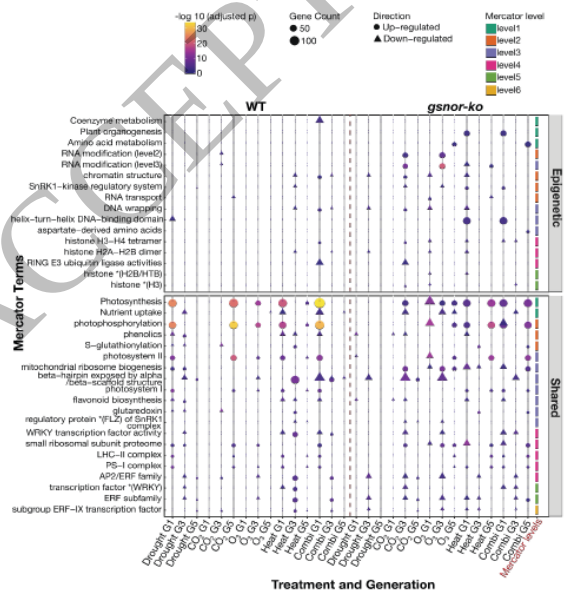
**Fig 3. Global transcriptome structure, differential expression, and intergenerational overlap in WT and *gsnor-ko*. (A)** Discriminant analysis of principal components (DAPC) of VST-transformed RNA-seq data for WT and *gsnor-ko* across generations G1, G3, and G5. Symbols indicate generations and colours indicate treatments (Control, Drought, $CO_2$, $O_3$, Heat, and Combination). LD1 and LD2 represent the first two discriminant axes. CV indicates mean held-out classification accuracy ± standard deviation across 100 repeated, class-stratified train/test splits with a nominal training fraction of 80%. Each RNA-seq library represents one plant. Non-control groups contained four libraries per genotype × treatment × generation; control groups contained five, except WT G1, which contained six. **(B)** Numbers of up-regulated and down-regulated differentially expressed genes (DEGs) for each treatment and generation in WT and *gsnor-ko*. Up-regulated genes are shown in red and down-regulated genes in blue. DEGs were identified using DESeq2 with Benjamini–Hochberg-adjusted $P < 0.05$. Each comparison used the corresponding genotype- and generation-matched control. G5 indicate treatment history. Three-generation overlap was evaluated using 20,000 random-set permutations, with Benjamini–Hochberg correction across ten genotype × treatment comparisons; complete results are provided in Supplementary File S23. **(C)** Venn diagrams showing overlap of DEG sets among G1, G3, and G5 within each treatment for WT and *gsnor-ko*. Numbers indicate the number of unique and shared DEGs across generations. Combi, combination treatment. **ALT TEXT:** Discriminant plots, differential gene counts, and overlap diagrams show treatment- and generation-specific transcriptome responses that differ between wild type and *gsnor* knockout.




ACCEPTED MANUSCRIPT

Downloaded from academic.oup.com/jxb/advance-article/doi/10.1093/jxb/erag557/9016158 by guest on 12 November 2026

**Fig. 4. Selected epigenetic-associated and shared recurrent Mercator enrichment signatures in WT and *gsnor-ko*.** Mercator enrichment of upregulated and downregulated DEGs was analysed separately for each genotype × treatment × generation comparison using clusterProfiler's enricher function with Benjamini–Hochberg correction. DEGs were defined by adjusted $P < 0.05$ without a minimum absolute $\log_2$ fold-change cutoff. For each contrast and annotation level, the background comprised genes with non-missing adjusted P-values and $\log_2$ fold changes that were represented in the retained Mercator categories; categories containing 10–500 eligible genes were tested. Enrichment used pvalueCutoff = 0.05 and qvalueCutoff = 0.20; the plotting script additionally retained entries with unadjusted $P \leq 0.05$ and Benjamini–Hochberg-adjusted $P \leq 0.20$. The upper panel displays enrichment results for a set of epigenetically associated categories. The lower panel displays other categories enriched in at least two of G1, G3, and G5 in at least one treatment for each genotype. The qualifying treatment could differ across genotypes, and recurrence did not require enrichment in the same direction of expression. All qualifying occurrences of the selected shared categories are displayed. Symbol size indicates the number of input DEGs assigned to each category, and colour indicates $-\log_{10}$(Benjamini–Hochberg-adjusted P). Circles represent enrichment among upregulated genes and triangles among downregulated genes. The annotation strip identifies the Mercator hierarchy level. RNA-seq groups contained four plant-derived libraries per non-control group and five per control group, except WT G1 control, which contained six. G5 indicate treatment history. Combi, combination treatment. **ALT TEXT:** Bubble plots show recurrent enrichment of chromatin, epigenetic, photosynthetic, redox, and stress related functions across treatments and generations in both genotypes.




ACCEPTED MANUSCRIPT

Downloaded from academic.oup.com/jxb/advance-article/doi/10.1093/jxb/erag557/9016158 by guest on 12 November 2026

**Fig 5. Proposed epigenetic models linking repeated climate stress and altered redox status to multi-generational transcriptional persistence.** Schematic representation of five non-mutually exclusive mechanistic models derived from the transcriptomic analyses and the known functions of candidate regulators. **(A)** DNA methylation and heterochromatin reinforcement via RNA-directed DNA methylation (RdDM) and chromatin compaction pathways, including Pol IV, RDR2, DCL3, AGO6, DRM2, CMT3, DMS3/DRD1/RDM1, DDM1, H2A.W, MORC3/6, and ADCP1; Created in BioRender. Lindermayr C (2026) https://BioRender.com/8el21jp. **(B)** Polycomb-linked repression and chromatin stabilisation, in which BPC proteins may contribute to PRC2 recruitment (including MSI1), leading to H3K27me3-associated silencing and reinforcement through LHP1-MSI1; Created in BioRender. Lindermayr C (2026) https://BioRender.com/16ng2z9. **(C)** Dynamic regulation of histone H2B ubiquitination through HUB1/2-mediated deposition and deubiquitination via the UBP22-SGF11-ENY2 module, potentially linked to DET1-dependent chromatin resetting; Created in BioRender. Lindermayr C (2026) https://BioRender.com/e6ikx1y. **(D)** RNA methylation-based regulation, in which FIP37 and ALKBH10B may influence mRNA stability, processing, translation, and stress-response output. **(E)** One-carbon and methyl-donor metabolism, where SAMS4 and related pathways may affect S-adenosylmethionine availability and thereby influence DNA/histone methylation and stable repression. These models represent working hypotheses and, by themselves, do not demonstrate direct epigenetic inheritance; Created in BioRender. Lindermayr C (2026) https://BioRender.com/cir2ibe. These literature-informed schematics represent candidate mechanisms; the depicted chromatin and RNA modifications were not directly measured in this study. **ALT TEXT:** Schematic of five candidate regulatory models linking redox imbalance to DNA methylation, Polycomb repression, histone ubiquitination, RNA methylation, and one carbon metabolism.

ACCEPTED MANUSCRIPT

Downloaded from academic.oup.com/jxb/advance-article/doi/10.1093/jxb/erag557/9016158 by guest on 12 November 2026

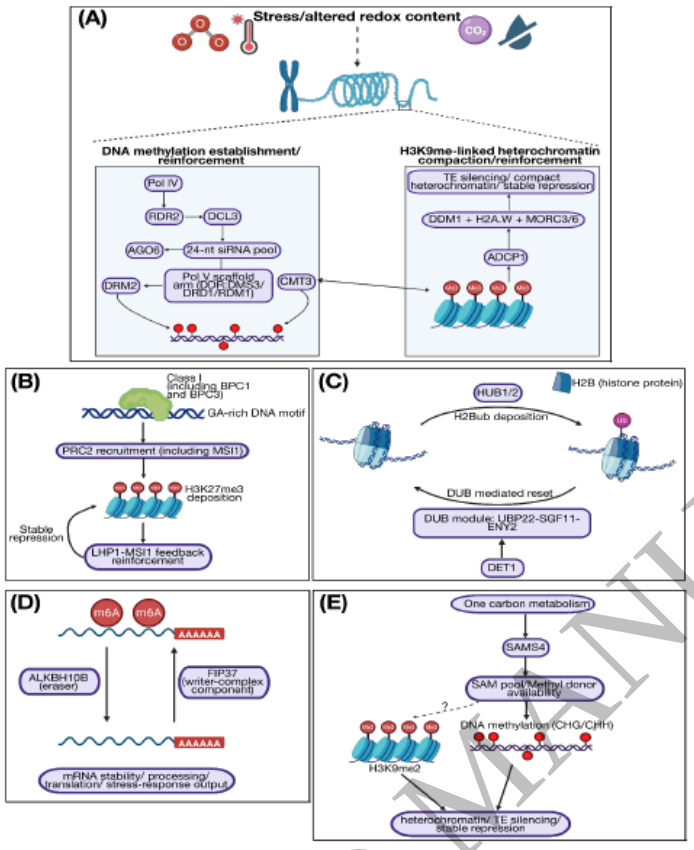
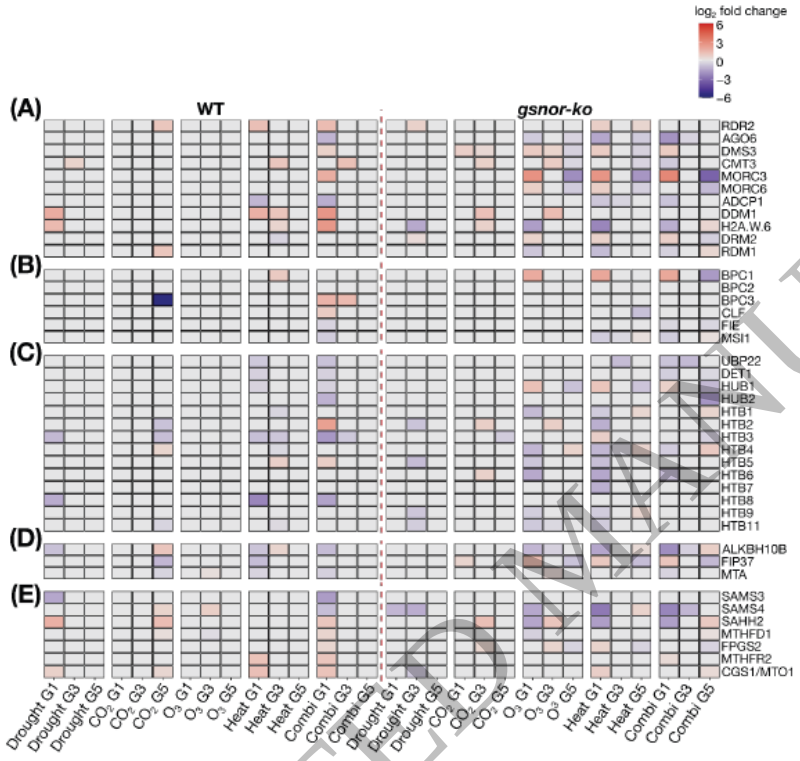



**Fig. 6. Differential expression of candidate chromatin-, RNA- and methyl-donor-associated regulators in WT and *gsnor-ko*.** Heatmaps show selected candidate genes associated with the five proposed regulatory models across drought, elevated $CO_2$, elevated $O_3$, heat and combination treatments in G1, G3 and G5. (A) DNA methylation, RNA-directed DNA methylation and heterochromatin-associated genes. (B) Polycomb- and chromatin repression-associated genes. (C) Histone H2B ubiquitination and chromatin resetting-associated genes. (D) RNA methylation-associated genes. (E) One-carbon metabolism and methyl-donor-associated genes. Genes were specified using manually curated Arabidopsis gene identifiers. Each cell represents a DESeq2 $\log_2$ fold-change estimate relative to the corresponding genotype- and generation-matched control. Estimates are coloured only when the Benjamini–Hochberg-adjusted P-value is $< 0.05$; no minimum absolute $\log_2$ fold-change cutoff was applied. Red indicates upregulation and blue indicates downregulation, with colour intensity indicating effect size. The colour scale is capped at ±6. Nonsignificant results and unavailable fold-change estimates were assigned zero for plotting and appear grey; grey therefore does not establish unchanged expression. The dashed vertical line separates WT and *gsnor-ko*. Non-control groups contained four plant-derived RNA-seq libraries; control groups contained five, except WT G1 control, which contained six. G5 indicate treatment history. Candidate grouping reflects

ACCEPTED MANUSCRIPT

Downloaded from academic.oup.com/jxb/advance-article/doi/10.1093/jxb/erag557/9016158 by guest on 12 November 2026

published functions rather than direct measurement of the proposed regulatory mechanisms. Combi, combination treatment. **ALT TEXT:** Heatmaps show treatment and generation dependent expression of candidate epigenetic regulators, revealing distinct expression patterns between wild type and *gsnor* knockout.

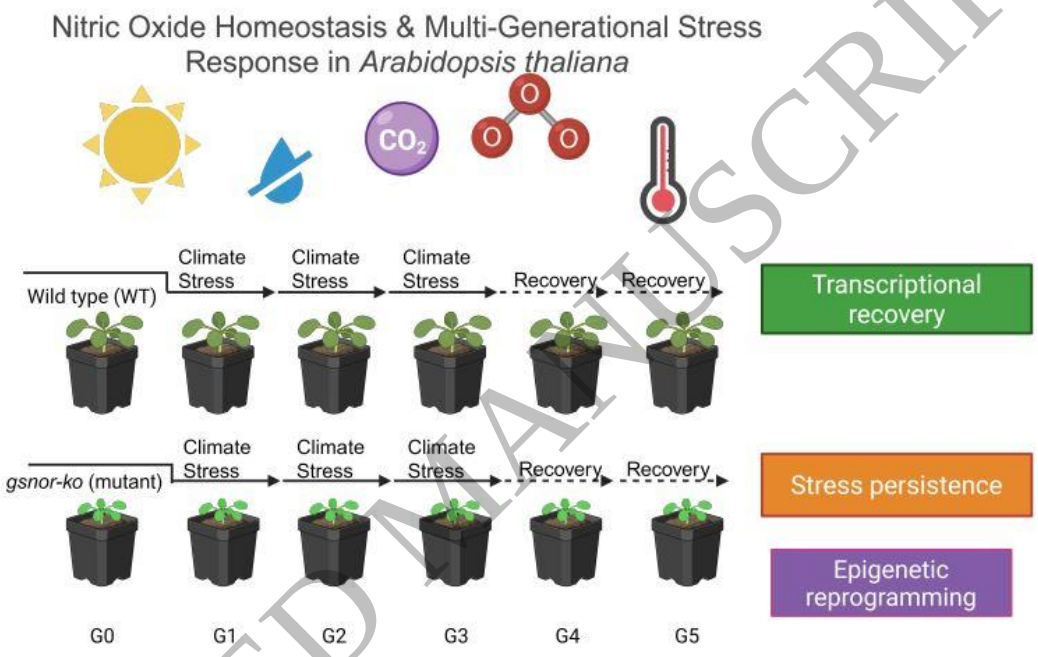



ACCEPTED MANUSCRIPT

Downloaded from academic.oup.com/jxb/advance-article/doi/10.1093/jxb/erag557/9016158 by guest on 12 November 2026

## Graphical abstract

**ALT TEXT:** Repeated climate stress is followed by transcriptomic recovery in wild type Arabidopsis, whereas impaired nitric oxide homeostasis is associated with stress persistence and epigenetic reprogramming.




ACCEPTED MANUSCRIPT

Downloaded from academic.oup.com/jxb/advance-article/doi/10.1093/jxb/erag557/9016158 by guest on 12 November 2026